# The tempo of cetacean cranial evolution

Ellen J. Coombs, Ryan N. Felice, Julien Clavel, Travis Park, Rebecca Bennion, Morgan Churchill, Jonathan H. Geisler, Brian Beatty, Anjali Goswami

▶ **To cite this version:**

Ellen J. Coombs, Ryan N. Felice, Julien Clavel, Travis Park, Rebecca Bennion, et al.. The tempo of cetacean cranial evolution. Current Biology - CB, 2022, 32 (10), pp.2233-2247. 10.1016/j.cub.2022.04.060 . hal-03666596

**HAL Id: hal-03666596**
**https://hal.science/hal-03666596**

Submitted on 27 Oct 2022

**HAL** is a multi-disciplinary open access archive for the deposit and dissemination of scientific research documents, whether they are published or not. The documents may come from teaching and research institutions in France or abroad, or from public or private research centers.

L'archive ouverte pluridisciplinaire **HAL**, est destinée au dépôt et à la diffusion de documents scientifiques de niveau recherche, publiés ou non, émanant des établissements d'enseignement et de recherche français ou étrangers, des laboratoires publics ou privés.

Article

Current Biology

# The tempo of cetacean cranial evolution

## Highlights

- Cetacean diversity was obtained through three key periods of rapid evolution
- Highest evolutionary rates are seen during the initial evolution of stem whales
- High evolutionary rates occur as neocetes diverge, and later as odontocetes diversify
- Diet and echolocation have the strongest influence on cranial morphology

## Authors

Ellen J. Coombs, Ryan N. Felice, Julien Clavel, ..., Jonathan H. Geisler, Brian Beatty, Anjali Goswami

## Correspondence

ellen.coombs.14@ucl.ac.uk

## In brief

Coombs et al. quantify morphology, disparity, and evolutionary rates in the cetacean cranium. Highest evolutionary rates are seen during the initial evolution of stem whales, followed by high rates at the divergence of neocetes and later the diversification of odontocetes. Diet and echolocation have the strongest influence on cranial morphology.

Coombs et al., 2022, Current Biology *32*, 2233–2247
May 23, 2022 © 2022 The Authors. Published by Elsevier Inc.
https://doi.org/10.1016/j.cub.2022.04.060

CellPress

Current Biology

CellPress
OPEN ACCESS

Article

# The tempo of cetacean cranial evolution

Ellen J. Coombs,[1,2,9,10,*] Ryan N. Felice,[3] Julien Clavel,[4] Travis Park,[2] Rebecca F. Bennion,[5,6] Morgan Churchill,[7] Jonathan H. Geisler,[8] Brian Beatty,[8] and Anjali Goswami[2]

[1]Division of Biosciences, Department of Genetics, Evolution & Environment, University College London, Gower Street, London WC1E 6BT, UK
[2]Department of Life Sciences, Natural History Museum, Cromwell Road, London SW7 5BD, UK
[3]Division of Biosciences, Cell & Developmental Biology, University College London, Gower Street, London WC1E 6BT, UK
[4]Univ Lyon, Université Claude Bernard Lyon 1, CNRS, ENTPE, UMR 5023 LEHNA, 69622 Villeurbanne, France
[5]Evolution & Diversity Dynamics Lab, Université de Liège, Liège, Belgium
[6]OD Earth and History of Life, Royal Belgian Institute of Natural Sciences, Brussels, Belgium
[7]Department of Biology, University of Wisconsin Oshkosh, 142 Halsey Science Center, 800 Algoma Boulevard, Oshkosh, WI 54901, USA
[8]Department of Anatomy, College of Osteopathic Medicine, New York Institute of Technology, Old Westbury, NY 11568, USA
[9]Twitter: @ellencoombs
[10]Lead contact
*Correspondence: ellen.coombs.14@ucl.ac.uk
https://doi.org/10.1016/j.cub.2022.04.060

## SUMMARY

The evolution of cetaceans (whales and dolphins) represents one of the most extreme adaptive transitions known, from terrestrial mammals to a highly specialized aquatic radiation that includes the largest animals alive today. Many anatomical shifts in this transition involve the feeding, respiratory, and sensory structures of the cranium, which we quantified with a high-density, three-dimensional geometric morphometric analysis of 201 living and extinct cetacean species spanning the entirety of their ~50-million-year evolutionary history. Our analyses demonstrate that cetacean suborders occupy distinct areas of cranial morphospace, with extinct, transitional taxa bridging the gap between archaeocetes (stem whales) and modern mysticetes (baleen whales) and odontocetes (toothed whales). This diversity was obtained through three key periods of rapid evolution: first, the initial evolution of archaeocetes in the early to mid-Eocene produced the highest evolutionary rates seen in cetaceans, concentrated in the maxilla, frontal, premaxilla, and nasal; second, the late Eocene divergence of the mysticetes and odontocetes drives a second peak in rates, with high rates and disparity sustained through the Oligocene; and third, the diversification of odontocetes, particularly sperm whales, in the Miocene (~18–10 Mya) propels a final peak in the tempo of cetacean morphological evolution. Archaeocetes show the fastest evolutionary rates but the lowest disparity. Odontocetes exhibit the highest disparity, while mysticetes evolve at the slowest pace, particularly in the Neogene. Diet and echolocation have the strongest influence on cranial morphology, with habitat, size, dentition, and feeding method also significant factors impacting shape, disparity, and the pace of cetacean cranial evolution.

## INTRODUCTION

The evolution of cetaceans (whales, dolphins, and porpoises) involves one of the most extreme transitions of any vertebrate lineage.[1,2] This shift occurred over an evolutionarily short 8–12 million years[2,3] and is captured by an exceptional fossil record beginning in the early Eocene (~53 Ma[2]) that documents the reorganization of the cetacean body into that of a fully aquatic organism. Some of the most extreme anatomical changes in this transition occurred in the skull, allowing whales to feed, breathe, and navigate in their new aquatic environments.

The anatomical restructuring of the cetacean skull began with the archaeocetes, a paraphyletic assemblage of stem cetaceans[2] that bridges the transition from terrestrial ancestors to fully aquatic taxa.[4] The earliest archaeocetes, pakicetids (ca. 53–47 Mya, Indo-Pakistan[2]), bore nasals at the tip of their rostrum, similar to terrestrial artiodactyls,[5] and were capable of normal terrestrial locomotion. Nonetheless, they had also already begun to adapt to an aquatic lifestyle, subsisting on freshwater prey[5] and evolving pachyosteosclerotic tympanic bullae surrounding the external part of the ear canal.[6]

Crown cetaceans, the neocetes, appeared ~39 Mya[7] (late Eocene) and are clearly differentiated from archaeocetes by additional cranial autapomorphies, including cranial telescoping. This shifting results in a foreshortening of the posterior skull and accommodates easier breathing at the water's surface,[8–11] an important adaptation for an aquatic lifestyle.

Neocetes are differentiated into the two modern suborders: the baleen whales (mysticetes) and the toothed whales (odontocetes). Mysticetes evolved large body sizes and specializations, such as baleen, for several mass feeding strategies,[1,12] while odontocetes evolved echolocation (biosonar) for navigation, hunting, and interaction with congeners.[13–15] These two vastly different strategies have resulted in distinctive adaptations of the skull,[1,2] which, due to its morphological and functional complexity, is highly informative for understanding and


This is an open access article under the CC BY license (http://creativecommons.org/licenses/by/4.0/).

reconstructing cetacean biology and evolution.[1,2] Extant mysticetes are characterized by a dorsoventrally flattened rostrum, posterior extension of the palate, prograde telescoping, and baleen. In contrast, the odontocete skull typically shows asymmetry in the naso-facial region, a consequence of asymmetry in the overlying soft tissues that relates to the ability to echolocate,[1,8,16,17] retrograde cranial telescoping,[9] and homodont or reduced dentition.

To date, work on cetacean macroevolution has largely focused on one or the other suborders, or on radiations and diversification in neocetes.[7,18,19] Here, we conduct the first comprehensive study to reconstruct the drivers of shape variation, disparity (morphological diversity), and evolutionary rate in the cetacean cranium throughout their entire evolutionary history. To do so, we gathered the most expansive 3D scan dataset ever for Cetacea, spanning 88 living species (representing ~95% of extant cetacean species[20]) and 113 fossil species. We extracted high-density 3D geometric morphometric data and used these to quantify morphology, disparity, and evolutionary rate of the cetacean cranium in unprecedented detail. Because the tetrapod cranium is known to evolve in a modular fashion, with individual skeletal elements exhibiting distinct evolutionary histories,[10,21,22] we characterized variation in the skull as a whole and in each skull element, identifying the major factors influencing shape and reconstructing evolutionary rates and disparity over 50 million years of cetacean evolution. We hypothesize that (1) fossils demonstrate rapid transitions into novel morphospace, (2) echolocation and feeding strategies are primary drivers of cranial morphology, and (3) fast rates of evolution are associated with key innovations in these traits.

## RESULTS

### Cranial variation

Archaeocetes, mysticetes, and odontocetes occupy distinct areas of cranial morphospace (Figure 1), with early members of each extant clade bridging these regions (see Figure S1 for all species positions). PC1 accounts for 41.6% of skull shape variation and is dominated by change in the relative length of the rostrum. The negative end of PC1 represents the brachycephalic faces of suction-feeding species such as the Pliocene *Odobenocetops*, extant kogiids, and other snub-faced species such as *Orcaella* spp., as well as some phocoenids. The positive end of PC1 is occupied by dolichocephalic, long-snouted fish-eating species such as the extinct eurhinodelphinids and extant river dolphins.

PC2 accounts for 24.9% of total shape variation and predominantly reflects changes in the positioning of the nares. The negative end of PC2 is represented by early archaeocetes such as *Pakicetus* and *Ambulocetus*, which have anteriorly positioned nares, with Eocene and Oligocene specimens occupying more intermediate positions on this axis. The positive end of PC2 is occupied by later Miocene and extant odontocetes, which have nasals positioned high on the head. Cranial variation along the major axes is displayed in Figure 1, with maximum and minimum shape variation in each cranial bone provided in Figure S2.

Odontocetes occupy the largest region of morphospace, spanning the full range of PC1, in comparison to the other subclades. Extant odontocetes fill the upper left quadrant of the PC1-PC2 morphospace, which characterizes a mid-length rostrum, a bulbous cranium, and nares that have moved posteriorly on the skull. Miocene odontocetes such as the extremely dolichocephalic Eurhinodelphinidae and Allodelphinidae dominate the upper right quadrant (Figure 1). The central region of the morphospace is occupied by Oligocene odontocetes, which bridge the regions occupied by archaeocetes and later Miocene and extant odontocetes. Oligocene odontocetes in the center of the morphospace include squalodontids, patriocetids, and early diverging xenorophids, which have nares positioned slightly more anteriorly and still retain basal features such as heterodonty.[16]

Mysticetes occupy the positive end of PC1 and an intermediate position on PC2, a region defined by the characteristic mysticete elongation of the rostrum and the prograde telescoping of the nares. There is a clear division among mysticetes of different time periods. The Eocene *Mystacodon selenensis*, which is not only the oldest mysticete in this dataset but also the current oldest known neocete,[23,24] sits near to the Eocene archaeocetes, while Oligocene mysticetes, such as aetiocetids, bridge the space between archaeocetes and modern baleen whales.

The nares are further posteriorly positioned in mysticetes than in their archaeocete ancestors that occupy the lower right quadrant of the morphospace, reflecting the long rostra and anteriorly placed nasals of the latter. It is noteworthy that extinct toothed mysticetes and archaeocetes overlap substantially in this cranial morphospace.

### Patterns of cranial evolution through time and across Cetacea

A variable-rates lambda model (Lambda_var) had the best model fit for the entire skull and for all individual skull bones (Figure S3). Lambda was estimated as 0.69 for the whole skull, suggesting a moderately high level of phylogenetic signal. The highest evolutionary rates are observed within the archaeocetes (Figures 2 and S4), especially in Pakicetidae, Ambulocetidae, and Remingtonocetidae (Figure 3), throughout the mid-Eocene (Figure 2). This initial burst is followed by a second notable diversification at the end of the Eocene (~39–36 Mya), with the origin of Neoceti (Figure 2). This second burst of diversification involves the newly diverging mysticetes of the late Eocene and early Oligocene, including Mystacodontidae and Mammalodontidae, as well as the initial early Oligocene radiation of the simocetid and xenorophid odontocetes (Figure 3). Thereafter, high rates of evolution are observed in the odontocete superfamily Physeteroidea, which includes Physeteridae and Kogiidae (Figures 2 and 3), and in the early divergence of the eurhinodelphinids from Allodelphinidae, Squalodelphinidae, and Platanistidae (although rates rapidly slow down within the eurhinodelphinids in the mid-late Miocene; Figure 2). Some of the highest odontocete evolutionary rates are seen in the Pliocene Odobenocetopsidae, reflecting the unusual morphology of this taxon (Figure 3).

In the analyses of individual cranial elements, there are three key peaks in the rate of evolution across Cetacea, specifically in the late Eocene, the mid-late Oligocene, and to a lesser extent, the mid-Miocene (Figures 4A and 4B). The nasal shows high rates of evolution, particularly in the mid-late Eocene. The archaeocetes show a peak in maxilla, premaxilla, and nasal rates in the middle Eocene (Figure 4C). The flatline in the data

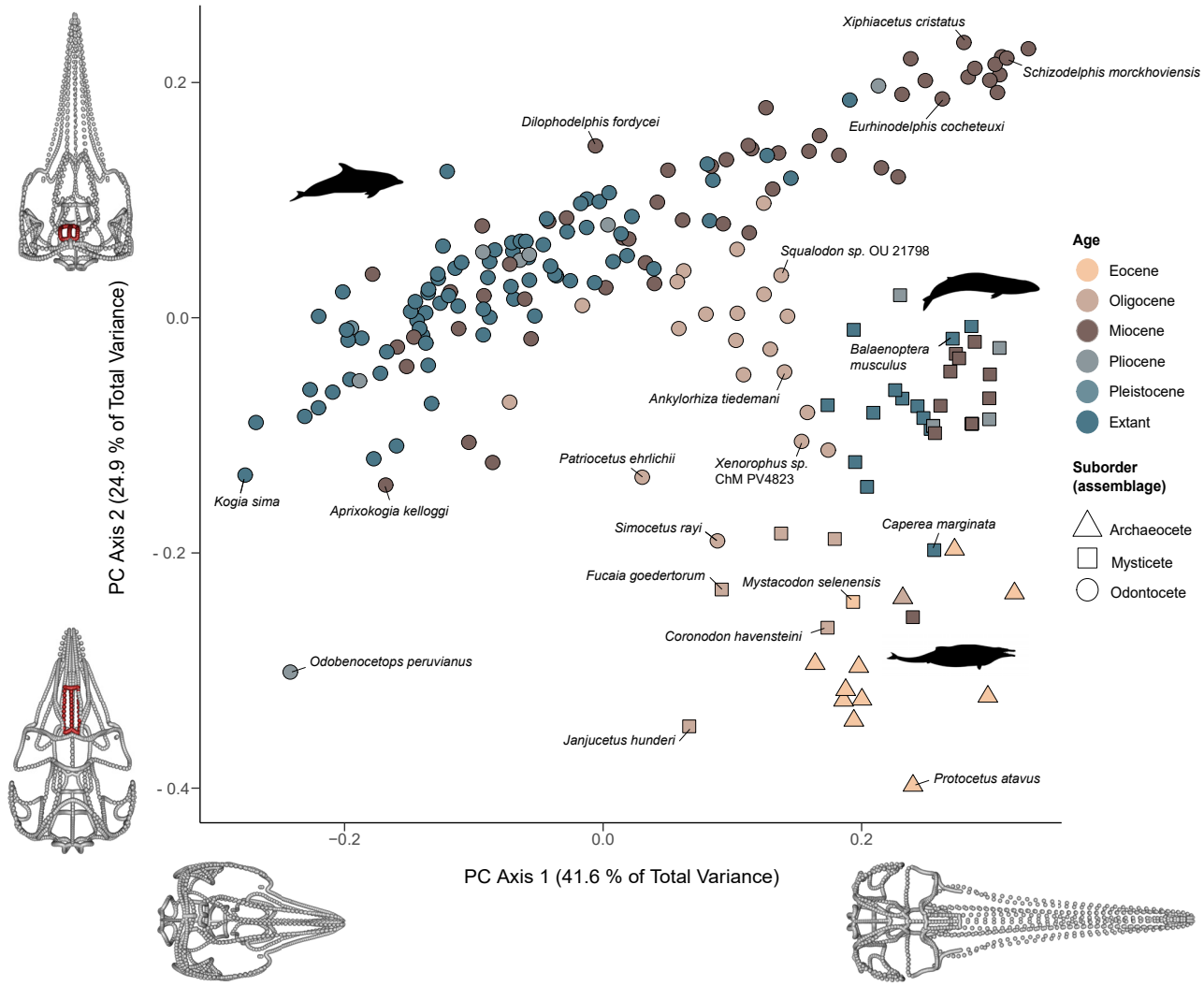


**Figure 1. Cetacean cranial morphospace showing estimated skull shapes for the positive and negative extremes**

Estimated skull shapes for the positive and negative extremes are shown along PC1 (41.6%) and PC2 (24.9%). PC1 is dominated by change in the relative length of the rostrum. PC2 reflects changes in the positioning of the nares (shown here in red for clarity). Specimens that represent the extreme morphologies along each axis are highlighted. Note how the earliest odontocete in the dataset (*Simocetus rayi*: early Oligocene) and the earliest mysticete (*Mystacodon selenensis*: late Eocene) occupy a position intermediate between the archaeocetes and the early odontocetes and mysticetes, respectively. Further, note the clustering of Eocene and Oligocene specimens and of morphologically similar Miocene and extant specimens, particularly in the mysticetes. For a morphospace labeled with species names, see Figure S1.

thereafter is due to there being only one archaeocete in the dataset (*Kekenodon*) that lived into the late Oligocene. The mysticetes show a peak in the evolutionary rates of several bones toward the end of the Eocene after the two suborders had diverged, with a further peak in the late Oligocene (Figure 4D). Thereafter, rates remain conservative. High evolutionary rates in the frontal, maxilla, and nasal are found on the branch leading to the earliest diverging odontocetes (Figure S5). As well as high rates in their early divergence, the odontocetes show several peaks in evolutionary rate (mostly in the maxilla, frontal, and nasal) in the mid-late Oligocene (Figure 4E), with smaller peaks in the Miocene.

A pairwise t test with Bonferroni correction[27] showed a significant difference between archaeocete and mysticete evolutionary rates ($p < 0.001$), archaeocete and odontocete rates ($p < 0.001$), and mysticete and odontocete rates ($p < 0.001$) (Figure S4). The family Odobenocetopsidae accounts for the highest evolutionary (log mean) rates in odontocetes, followed by the early diverging Xenorophidae, Simocetidae, and later, kogiids (Figure 3). Moderate to high rates are observed in the patriocetids and waipatiids of the Oligocene, with the lowest rates seen in the later Eurhinodelphinidae, Lipotidae, and Iniidae (Figure 3). The highest rates in the mysticetes are seen in the early diverging Mystacodontidae and Mammalodontidae, followed by Aetiocetidae, the last of the toothed mysticetes. The lowest rates are seen in the Balaenopteridae (Figure 3). The highest rates in the archaeocetes are in Ambulocetidae, Remingtonocetidae, and Protocetidae (note that the high rates to the right of the density peak in

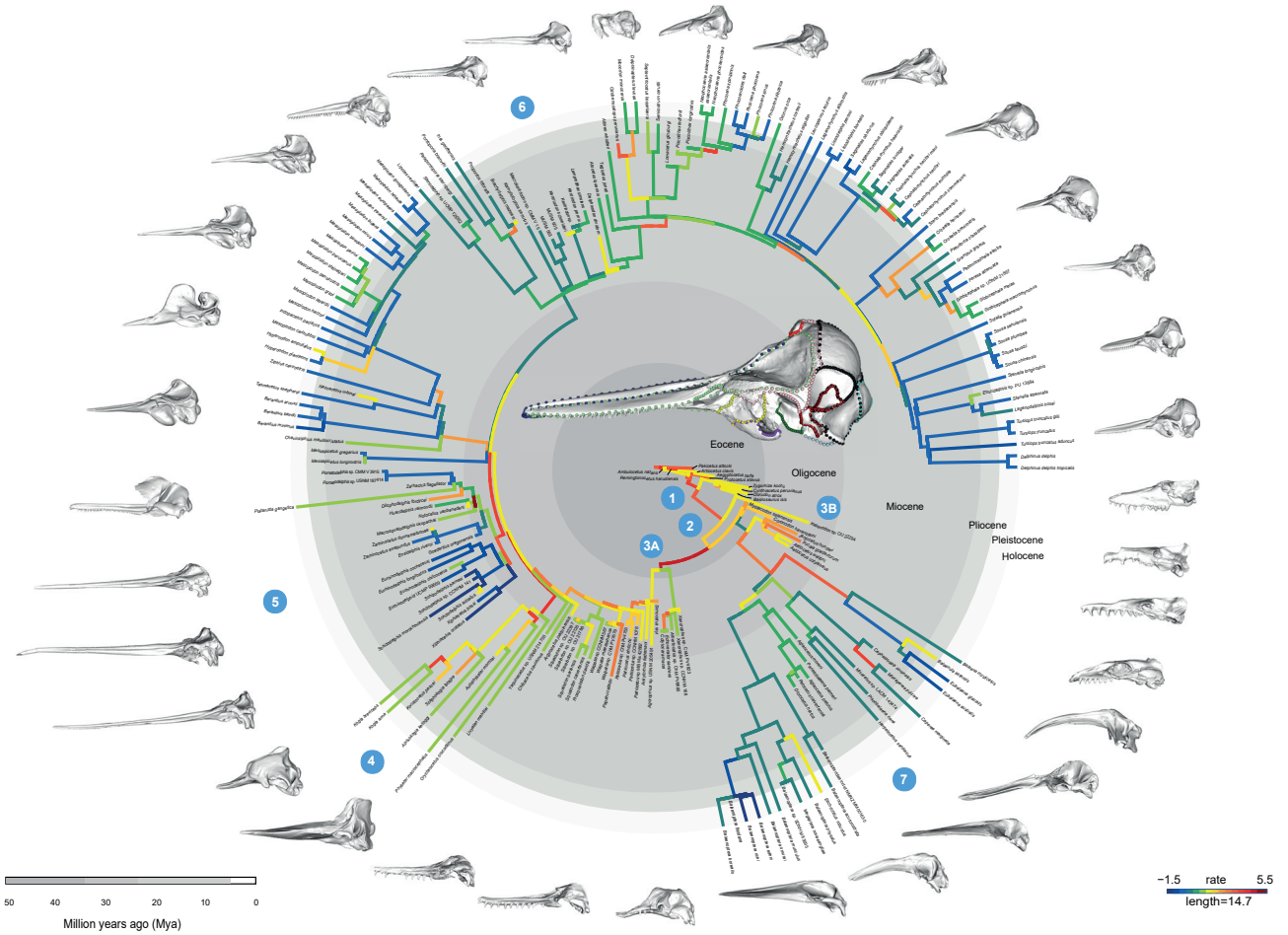


**Figure 2. Branch-specific rates of cranial evolution for Cetacea**

Rates modeled using a variable-rates Lambda model of evolution. A negative log-rate of evolution indicates a slowing down in the rate of trait change. (1) Archaeocetes, (2) the origin of Neoceti (~39–36 Mya), (3A) early diverging odontocetes, (3B) early diverging mysticetes, (4) Physeteroidea, (5) Eurhinodelphinidae, (6) extant odontocetes, and (7) extant mysticetes. Skull in the center shows an example of the landmark and curve configuration used throughout this study. A subset of the sampled skulls is figured, positioned proximal to their terminal branches to display the cranial diversity of living and extinct cetaceans. Gray scale bar (bottom left) shows million years ago (Mya); color scale bar (bottom right) shows rate of evolution with red and hotter colors indicating higher rates. See also Figure S5.

this family are obscured by Remingtonocetidae), while the lowest rates are seen in the Kekenodontidae (Figure 3).

We further quantified rates of evolution per suborder and per bone in mvMORPH[28] using the state-specific Brownian motion model (BMM) in the 'mvgls' function. Consistent with the BayesTraits results, archaeocetes showed the highest rates of evolution ($\sigma^2_{mult}$ = 123.02), followed by odontocetes ($\sigma^2_{mult}$ = 16.87) and mysticetes ($\sigma^2_{mult}$ = 15.91). Across the archaeocete skull, the highest evolutionary rates were seen in the maxilla, nasal, zygomatic (including squamosal), and frontal ($\sigma^2_{mult}$ = 53.64, 52.44, 34.98, and 30.76, respectively) (Figure 5A). The highest rates in odontocetes were observed in the nasal, premaxilla, and maxilla ($\sigma^2_{mult}$ = 16.14, 12.26, and 11.36, respectively) and in the mysticetes in the maxilla, zygomatic (including squamosal), and nasal ($\sigma^2_{mult}$ =14.60, 8.92, and 8.31, respectively) (Figure 5A). Mysticetes have the lowest rates across all bones except for the maxilla, jugal, mandibular process (including fossa), parietal, and zygomatic (with squamosal) (Figure 5A).

In contrast to the results for evolutionary rates, archaeocetes have the lowest disparity across the skull (measured as Procrustes variance [*pv*]; $pv = 1.68 \times 10^{-2}$). Disparity across the mysticetes and odontocete skull is higher: $pv = 5.84 \times 10^{-2}$ and $pv = 6.75 \times 10^{-2}$, respectively. The highest disparity is observed in the neocete frontal, maxilla, nasal, and premaxilla (Figure 5B). The archaeocete maxilla is the most disparate of the skull bones in these early whales ($pv = 3.27 \times 10^{-3}$), but disparity is much lower than that seen in the mysticete and odontocete maxilla ($pv = 1.36 \times 10^{-2}$ and $1.60 \times 10^{-2}$, respectively) (Figure 5B).

We further mapped the Procrustes distance from the mean skull shape across Cetacea to that of representative families to identify the primary regions of differentiation (Figure 6). The

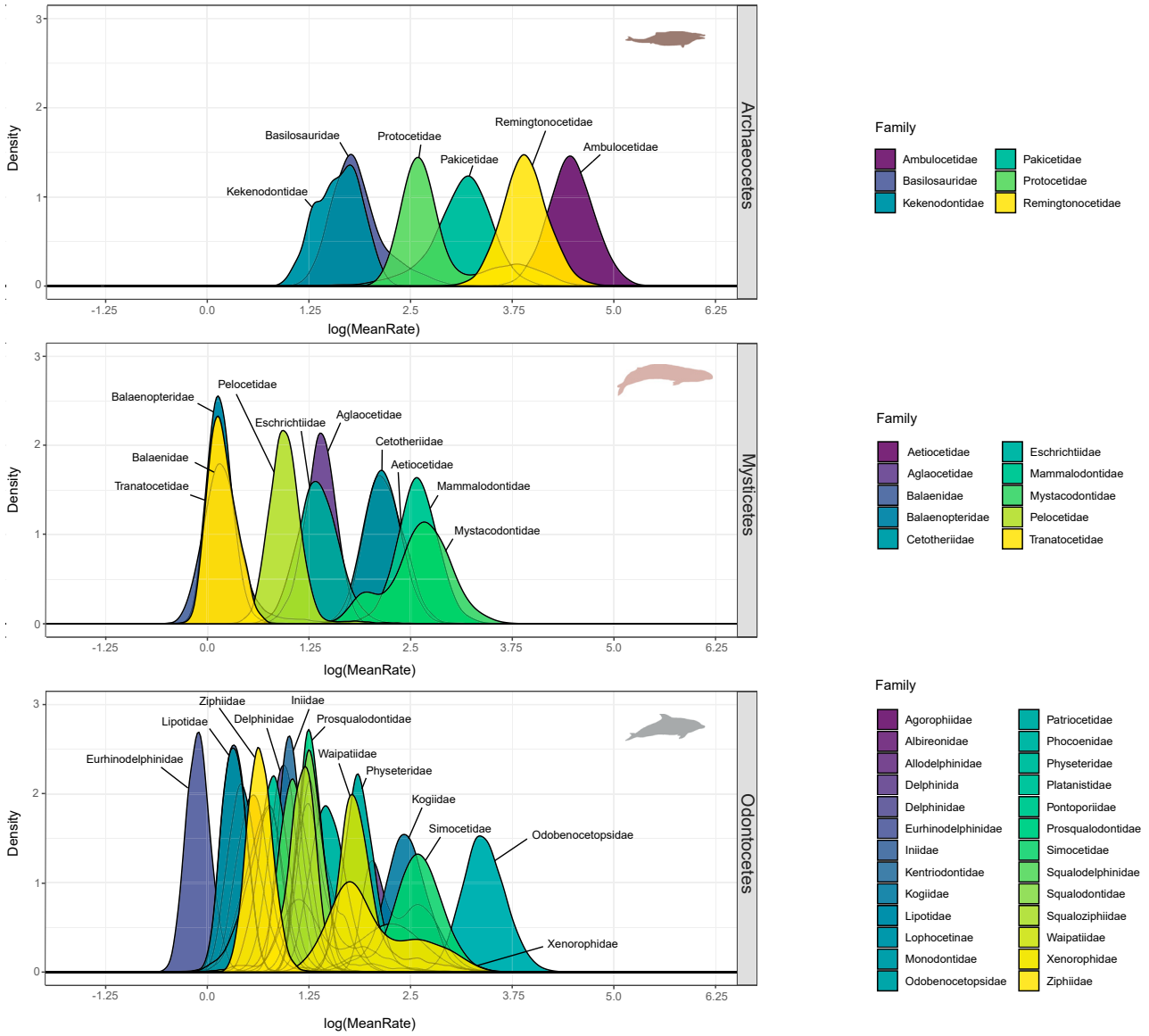


**Figure 3. Distribution of log mean rates of skull evolution for each cetacean group at the family level**

Rates shown for archaeocetes (top), mysticetes (middle), and odontocetes (bottom). Rates for terminal branches were extracted from the rjpp output from BayesTraits and binned by family. See also Figure S4.

predominant differences in Pakicetidae, Basilosauridae, and Protocetidae are concentrated in the positioning of the nares. Early mysticetes, such as the mammalodontids and aetiocetids, deviate from the mean skull shape mostly in the nares, while later mysticetes show higher deviation from the mean shape along the whole length of the premaxilla and maxilla from the antorbital and lateral processes of these bones to the tip of the rostrum. The early odontocetes (represented by Xenorophidae, Patriocetidae, and Squalodontidae) do not exhibit marked deviation from the mean shape, but in later odontocetes, there is high family-specific variation from the mean skull shape (Figure 6). *Odobenocetops* in particular deviates extensively from the mean skull shape over most of the skull (Figure 6) and occupies a unique area of the morphospace (Figure 1). In the eurhinodelphinids and some extant river dolphin families (Lipotidae, Iniidae, and Platanistidae), variation from the mean specimen is highest in the rostrum, which is highly elongated in these families, but not in some pontoporiids such as *Brachydelphis mazeasi*. Generally, in odontocetes high variation from the mean in extant families is concentrated in the naso-facial region and is particularly high in the delphinids and monodontids (Figure 6).

## Ecological influences on cranial evolution

Phylogenetic MANOVAs of whole skull shape variation supported significant associations of cranial shape with type of dentition, main diet component, echolocation ability, feeding method, and habitat. After correction for false discovery rate

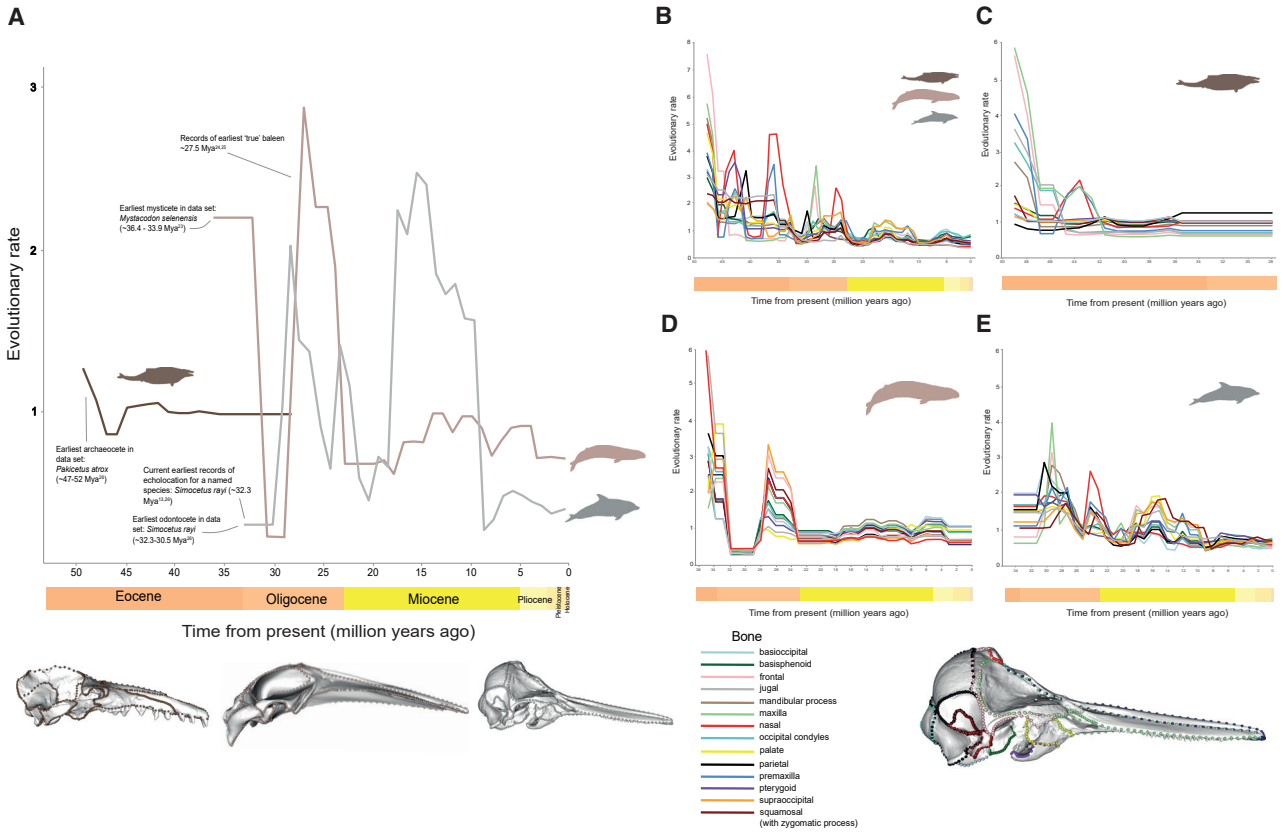


**Figure 4. Evolutionary rates through time per bone and across the entire skull for Cetacea and each suborder (assemblage)**

Evolutionary rates in the cetacean skull with a Lambda model and variable rates of evolution. The y axis shows evolutionary rate; the x axis shows time from present (million years ago).

(A) Average evolutionary rates across the whole skull for archaeocetes (dark brown), mysticetes (light brown), and odontocetes (gray). Landmarks and semi-landmarks shown on (L-R) *Aegyptocetus tarfa* MSNTUP I-15459, *Balaenoptera acutorostrata* NHM 1965.11.2.1, and *Delphinus delphis* AMNH 75332.

(B–E) Evolutionary rates per bone. (B) For all cetaceans in this dataset, (C) for archaeocetes, (D) for mysticetes, and (E) for odontocetes. Cetacea (B) are represented on a different scale from the suborders (C–E). This was so that details in the suborder plots, which were lost on a larger scale, could be easily viewed. Note: evolutionary models were run separately for Cetacea and each of the suborders. This means (B) is not a summation of (C)–(E), models do not capture the changes between groups, and the scaling in each analysis is different.

References from Geisler et al.,[13,24,25] Lambert et al.,[23] and Tsai and Fordyce.[26]

using the Benjamini-Hochberg method,[29,30] diet (effect size [es] = 4.51, $p < 0.001$), echolocation (es = 4.18, $p < 0.001$), dentition (es = 3.29, $p < 0.001$), size (es = 2.98, $p < 0.001$), feeding (es = 2.63, $p < 0.008$), and habitat (es = 2.11, $p < 0.02$) have a significant effect on skull shape. Finally, allometry is a significant, albeit relatively small, contributor to skull shape variation ($p < 0.001$, $r^2 = 0.15$, $F = 35.70$).

Rates of evolution also differ among ecological categories. Among dentition categories, heterodont cetaceans, such as the archaeocetes and early diverging neocetes, display the highest rates of evolution compared to lineages with other types of dentition ($\sigma^2_{mult} = 109.95$). Generally, the lowest evolutionary rates for the whole skull and individual bones belong to the "reduced" dentition feeders and the baleen feeders, with the exception of the maxilla, mandibular process, and zygomatic (including squamosal). These three elements display the second highest rates (of all the dentition categories) in baleen whales ($\sigma^2_{mult} = 13.04$, 6.38, and 5.78, respectively), although they remain substantially lower than rates observed in heterodont whales (Figure 7A).

When categorized by diet, the highest evolutionary rates ($\sigma^2_{mult}$) are seen in cetaceans that feed predominantly on benthic invertebrates and fish ($\sigma^2_{mult} = 131.98$), such as archaeocetes and early diverging neocetes. The lowest evolutionary rates are seen in cetaceans that feed on zooplankton and fish ($\sigma^2_{mult} = 11.82$), i.e., baleen whales. A similar pattern is also observed when individual bones are analyzed separately (Figure 7C). Compared to other dietary categories, cetaceans that feed on benthic invertebrates and fish have high rates of evolution in the nasal, parietal, premaxilla, and maxilla ($\sigma^2_{mult} = 53.40$, 51.17, 45.70, and 42.98, respectively). High evolutionary rates are also seen in the nasal of species that feed on tetrapods and fish ($\sigma^2_{mult} = 50.82$). This group includes basilosaurids, which show marked retrograde movement of the nares; the Oligocene *Ankylorhiza tiedemani*, the first large macrophagous odontocete that reoccupied the niche vacated by basilosaurids;[31] and the Miocene *Livyatan melvillei*, another macrophagous odontocete analogous with modern killer whales (*Orcinus orca*).[32] The lowest evolutionary rates per bone generally belong

CellPress
OPEN ACCESS

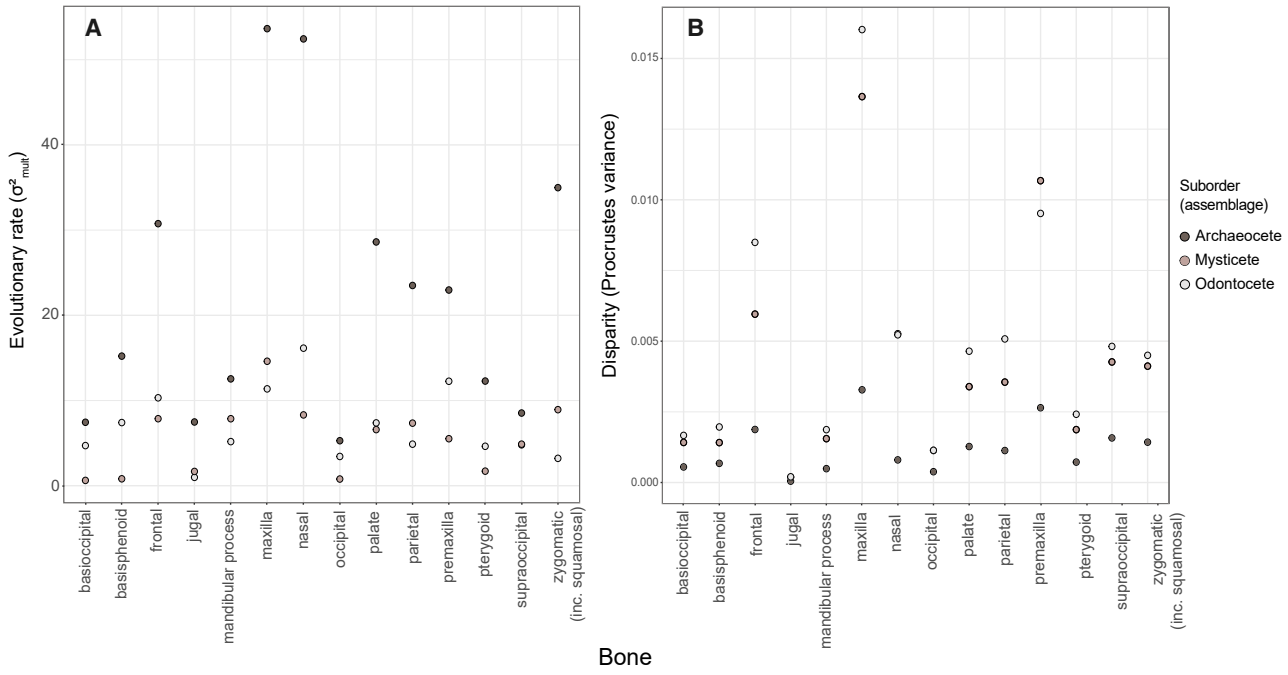


**Figure 5. Evolutionary rate and disparity per bone for each suborder (assemblage)**

(A) Evolutionary rate ($\sigma^2_{mult}$) per bone for each suborder (assemblage).

(B) Disparity (Procrustes variance) per bone, per suborder (assemblage). Disparity calculated using the whole cetacean dataset. Archaeocetes (dark brown), mysticetes (light brown), and odontocetes (light gray).

to zooplankton and fish feeders and cephalopod and fish feeders, with piscivores mostly displaying intermediate rates (Figure 7C).

Evolutionary rates also differ between echolocating and non-echolocating groups. Evolutionary rates are generally higher in cetaceans that cannot echolocate (archaeocetes, mysticetes, and the odontocete, *Odobenocetops*), with some exceptions. Rates are highest in the maxilla ($\sigma^2_{mult}$ = 22.43), nasal ($\sigma^2_{mult}$ = 20.25), and zygo-squamosal ($\sigma^2_{mult}$ = 16.64) of non-echolocating cetaceans, and highest in the frontal ($\sigma^2_{mult}$ = 11.96) and premaxilla ($\sigma^2_{mult}$ = 11.94) of echolocating odontocetes (Figure 7E).

Suction feeders, including, but not limited to, early mysticetes such as aetiocetids, most members of Physeteroidea (e.g., kogiids), ziphiids (beaked whales), and monodontids (narwhals and belugas), have the highest evolutionary rates ($\sigma^2_{mult}$ = 44.15). Filter feeders, which are all baleen-baring mysticetes and all Miocene or younger in age (in this study), generally have the lowest evolutionary rates across the skull ($\sigma^2_{mult}$ = 9.96) and in some individual bones (Figure S6A).

When separated by habitat, the highest rates across the skull are observed in cetaceans that live in coastal ($\sigma^2_{mult}$ = 29.74) and coastal-pelagic ($\sigma^2_{mult}$ = 27.78) environments, with the lowest rates seen in freshwater (riverine) inhabitants ($\sigma^2_{mult}$ = 0.49). Similar patterns are supported for individual bones, with some of the highest rates of evolution in the nasal (the highest at $\sigma^2_{mult}$ = 31.64 in coastal cetaceans), frontal, premaxilla, and maxilla of coastal and coastal-pelagic inhabitants and the lowest rates in the riverine taxa (Figure S6C). See additional supplemental information at https://github.com/EllenJCoombs/Cetacean_cranial_evolution for whole cranial rates, binned by ecological categories.

Differences in cranial disparity among ecological groupings largely, but not entirely, reflect patterns observed for evolutionary rates (Figure 7). When categorized by diet, no group is consistently more disparate across the whole skull; however, feeders on zooplankton and fish and benthic invertebrates and fish generally have some of the lowest levels of disparity in individual bones, and fish, cephalopod and fish eaters, and tetrapod and fish eaters tend to show some of the highest levels of disparity (Figure 7D). Echolocating cetaceans (the odontocetes except *Odobenocetops*) have the highest disparity across each bone, with lower disparity in taxa that do not echolocate (the archaeocetes and mysticetes) (Figure 7F). Finally, some of the highest disparity is observed in the skulls of pelagic cetaceans, which includes all ziphiids and some oceanic dolphins. The lowest disparity is seen in the bones of the skull of riverine cetaceans (Figure S6D), which comprises the three extant freshwater species in this study (*Inia geoffrensis*, *Lipotes vexillifer*, and *Platanista gangetica*). See additional supplemental information at https://github.com/EllenJCoombs/Cetacean_cranial_evolution for whole cranial disparity, binned by ecological categories.

## DISCUSSION

Cetaceans transitioned from being land-based to wholly aquatic in just 8 million years.[3] Here, we collected and analyzed the first morphometric dataset to quantify cetacean cranial morphology throughout their entire evolutionary history, spanning ~50 million years, to reconstruct the processes and factors that drove their

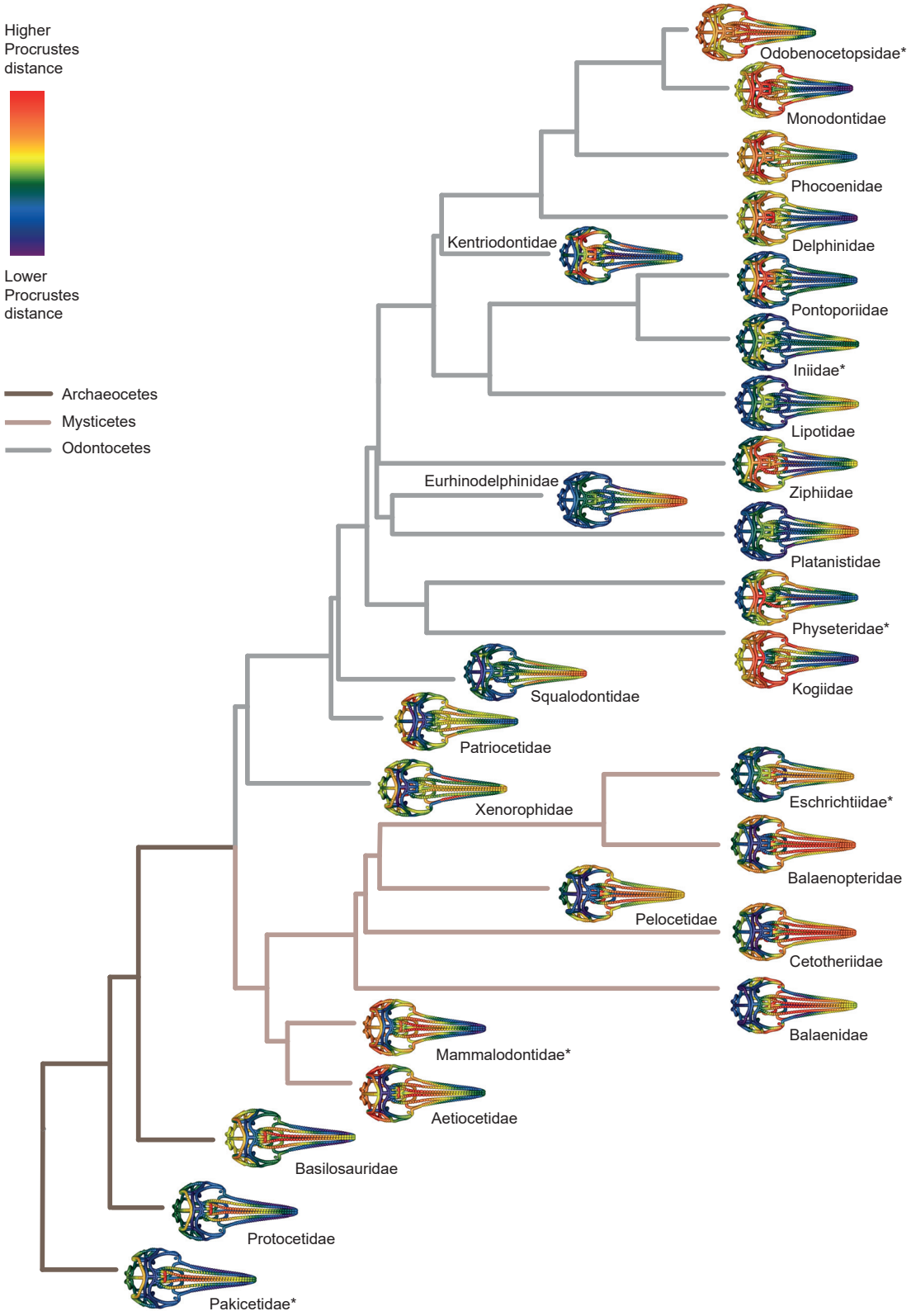


**Figure 6. Disparity across the skull in cetacean families**

Each depicted cranium displays the difference between mean skull shape for that family compared to the mean skull shape for Cetacea, with hotter colors indicating greater Procrustes distance (greater difference) in landmark positions. *Families represented by only one specimen in this dataset.

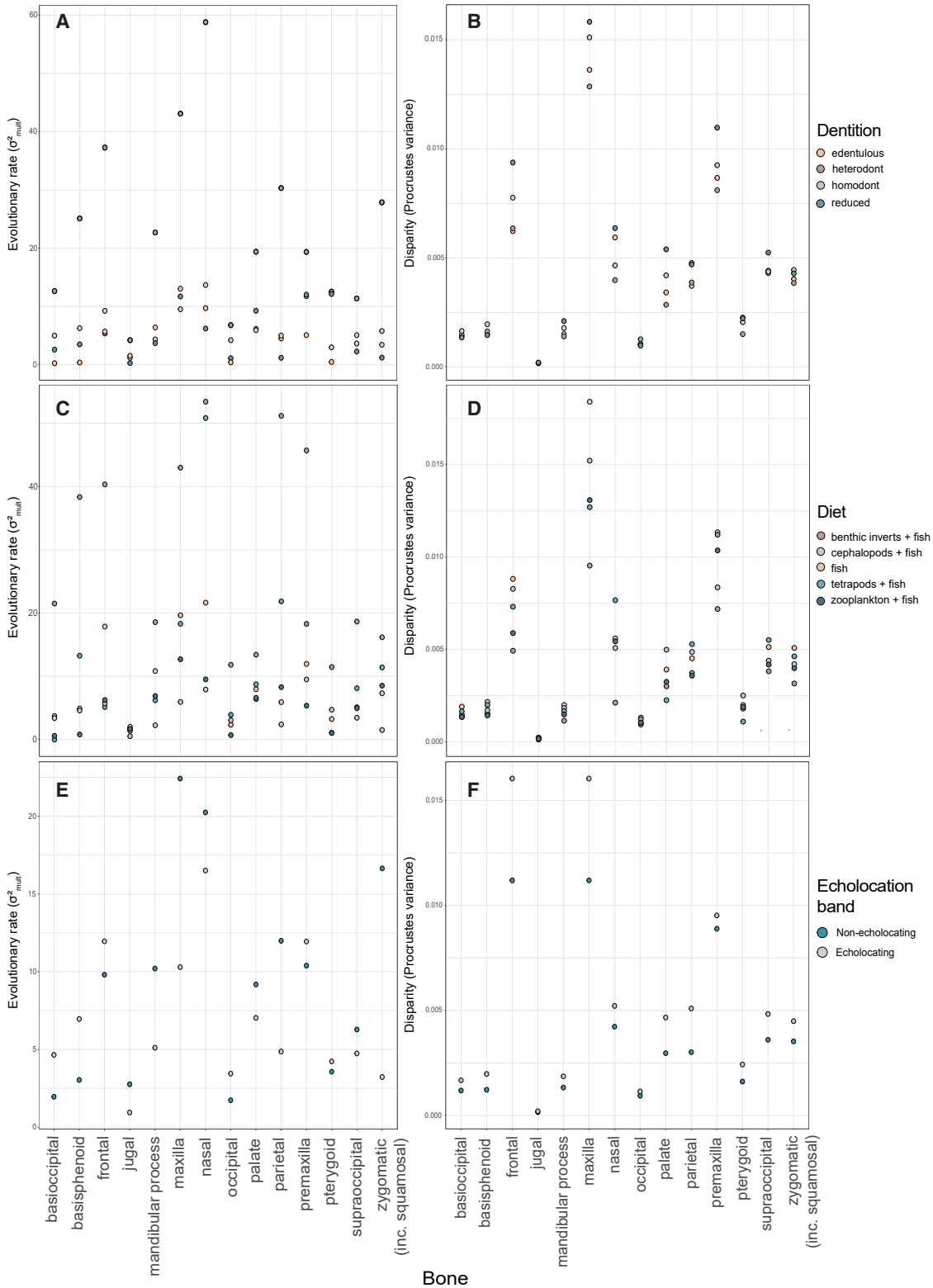


**Figure 7. Evolutionary rate and disparity per bone by dentition, diet, and echolocation ability**

Rates ($\sigma^2_{mult}$) calculated using the whole cetacean dataset.

(A) Evolutionary rates per dentition category: edentulous, heterodont, homodont, reduced.

(B) Disparity (Procrustes variance) per dentition category.

*(legend continued on next page)*

morphological diversification. Using high-dimensional landmark data to comprehensively represent the entire cranium for 201 living and fossil whales, we reconstructed the drivers of cranial shape variation, disparity, and evolutionary rates, recovering three key waves of morphological diversification that reflect the distinct ecological and evolutionary trajectories of the cetacean suborders.

### Early archaeocetes (~47.8–42 Mya)

Archaeocete cranial morphology evolved rapidly, both across the whole skull and in individual elements of the face (Figures 3, 4, and 5), possibly due to a lack of competition or to high productivity allowing or promoting rapid change.[33] Counterintuitively, archaeocetes show some of the lowest levels of cranial disparity. This rapid evolution without disparification is because despite archaeocetes having evolved rapidly to adapt to an aquatic lifestyle, they retained many plesiomorphic characteristics, such as heterodont dentition and no cranial telescoping.[2]

### Archaeocete to neocete transition (~39 Ma)

The origin of Neoceti in the late Eocene is followed by a sustained period of fast evolutionary rates, which continues into the mid-late Oligocene as the two suborders diverged into their distinct morphologies and niches. The pace of this diversification suggests that there were functional constraints early on in cetacean evolution that were overcome at or around the divergence of mysticetes and odontocetes. In odontocetes, high rates and disparity are associated with the rapid reorganization of the naso-facial region as they became increasingly specialized in their echolocation abilities. High disparity in the cranium in early mammalodontids (such as *Mammalodon*, which had the advantage of refined suction abilities[34]) suggests diversification and rapid occupation of their distinct niche with further adaptations to bulk (and later filter) feeding, consistent with patterns observed for mysticetes.[7]

### Odontocete specialization (Miocene)

The third wave of diversification in the cranium occurs in the Miocene and appears to be predominantly concentrated in odontocetes. Higher rates of cranial evolution throughout the Miocene can be attributed primarily to the Physeteroidea, likely associated with their highly specialized morphology, such as the supracranial basin, as well as with suction feeding. Several small peaks in evolutionary rates occur in odontocetes from 18 to 9 Mya, likely driven by smaller radiations in platanistoids and delphinids. Disparity is highest in Miocene odontocetes, with the cranium occupying the broadest range of the morphospace during this time as it diversified into a vast range of forms. In contrast, evolutionary rates and disparity remain conservative across contemporary mysticetes, with the exception of high rates observed during the early divergence of the balaenids and cetotheriids. Low rates of evolution thereafter may be a consequence of achieving an optimal morphology for their functional niche (filter feeding), as the mysticete skull and cranial disparity have not changed substantially in shape (in contrast to size) since the latest Oligocene.[7] This conservation of mysticete skull shape is evident in the clustering of Miocene to extant specimens in cranial morphospace (Figure 1).

Indeed, our high-resolution quantification of cranial shape demonstrates that each cetacean suborder occupies a distinct region in the morphospace (Figure 1) with some noteworthy overlap between early, toothed mysticetes and archaeocetes. For example, the earliest diverging mysticete, *Mystacodon selenensis* (late Eocene; 36.4 Ma[23,35]), lived alongside later archaeocetes such as *Kekenodon* and retained many basilosaurid-like features, such as a narrow rostrum. However, it also has a telescoped vertex and more posteriorly placed nares[35] seen in later mysticetes. Thereafter, morphologies associated with more crownward mysticetes start appearing, including an elongated rostral portion of the maxilla with a broad-based rostrum, as in *Janjucetus hunderi* (early Oligocene[34,36]), and later, a broader platyrostral skull and maxillae with thin lateral edges.[34,36]

There is a clear separation in the age of specimens, with Eocene archaeocetes, the Eocene mysticete, *Mystacodon selenensis*, and Oligocene neocetes overlapping in a similar region of the cranial morphospace. Baleen-bearing mysticetes cluster within a separate area of morphospace, with the exception of the highly autapomorphic clade of *Caperea* and *Miocaperea*, which fall closer to the stem cetaceans. Oligocene odontocetes, including xenorophids, patriocetids, waipatiids, and squalodontids, occupy an intermediate shape space between archaeocetes and extant odontocetes. These families all display poorly developed telescoping, more posteriorly placed nasals, and incipient asymmetry in the naso-facial region, a consequence of asymmetry in the overlying soft tissues that relates to the ability to echolocate.[8,16,17,] Echolocation in the odontocetes, both its evolution and refinement, is a defining characteristic of this suborder, enabling them to diversify into a vast range of forms[2] (Figure 1). Conversely, the morphology of mysticetes is likely constrained by the functional and morphological requirements of the dominant feeding strategies associated with an edentulous-baleen condition. These factors are reflected in the significant association of skull shape with diet, echolocation, dentition, feeding strategy, and habitat, as recovered in our analyses. Importantly, several of these factors have a greater effect than size; allometry explains around ~15% of skull shape variation across Cetacea, a similar value to that seen in close relatives and other marine mammals.[37–39]

Diet and echolocation have the strongest effects on cetacean skull variation and evolution, consistent with previous work linking prey size, diet type, feeding method, and echolocation with skull shape and diversity in odontocetes.[17,40–43] Mysticetes that feed on zooplankton and fish exhibit some of the lowest evolutionary rates across the skull and in most individual cranial bones (Figure 7). Additionally, this group also has the lowest disparity across the skull and consists entirely of filter and

(C) Evolutionary rates per diet category: fish, benthic invertebrates and fish, tetrapods and fish, and zooplankton and fish.
(D) Disparity per dietary category.
(E) Evolutionary rates for non- and echolocating groups.
(F) Disparity for non- and echolocating groups.
See also Figure S6.

suction-feeding mysticetes and one archaeocete: the late Oligocene *Kekenodon*, which likely fed raptorially and via filtration.[2]

When categorized by echolocation ability, cetaceans that cannot echolocate generally show higher rates of cranial evolution (Figure 7). This result is likely representative of the high evolutionary rates seen in the archaeocetes, early mysticetes such as *Mystacodon*, and the odontocete, *Odobenocetops* (Figures 2 and S5). Some exceptions to this pattern are observed in the premaxilla and frontal, which show higher rates of evolution in the echolocating odontocetes. Premaxillary rates are particularly high in the early divergences of Odontoceti and again in the early diverging Physeteroidea (mid-late Oligocene). These higher rates are likely due to changes in the face that accommodate echolocation.[17] In contrast to their fast rates of evolution, non-echolocating cetaceans display the lowest disparity. Odontocetes generally exhibit the highest disparity, reflecting an exceptional diversity in skull shape, with rostra that range from brachycephalic (e.g., *Odobenocetops* and *Kogia* spp.) to grossly elongate in dolichophallic species such as *Schizodelphis morckhoviensis*. Although likely linked to evolutionary rates, Sander et al.[44] reported that the evolution of echolocation, which allowed odontocetes to search for cephalopods while foraging at greater depths unavailable to early cetaceans lacking biosonar, is not directly coupled with evolution of size. In the present study, fish-eating odontocetes generally have the greatest disparity in analyses of individual skull bones, but this is closely followed by cephalopod and fish feeders and tetrapod and fish feeders. As suggested by Slater et al.,[43] a recent shift to a cephalopod diet in delphinids may explain an increase in body size disparity, consistent with the greater cranial disparity documented here. Sander et al.[44] identified feeding method as the driver of two major evolutionary pathways to large body size in cetaceans. Specifically, size evolution in odontocetes may be linked to raptorial feeding and deep-diving and, in the mysticetes, a loss of functional teeth in some lineages coupled with a switch of diet preference and the addition of bulk-feeding adaptations.[44]

When considering feeding method, suction-feeding whales exhibit many of the highest evolutionary rates in individual cranial bones (Figure S6A); this group includes the incipiently homodont Aetiocetidae,[45] the last of the toothed mysticetes. Many of these high rates are concentrated in the naso-facial region (in particular, the premaxilla, as well as the maxilla, nasal, and frontal) and, to a lesser extent, in the palatal portions. These high naso-facial rates appear to coincide with hypertrophy or elaboration of the soft facial tissues involved in phonation, as observed in Monodontidae and Physeteroidea (except for non-suction feeding sperm whales such as *Livyatan melvillei* and *Acrophyseter*)[32,46] (Figure S6A). Members of both families have heightened facial asymmetry in the premaxilla, maxilla, and where present, nasals.[17,47] Filter feeders, all of which are edentulous, baleen-bearing mysticetes, displayed the lowest evolutionary rates in individual cranial bones, with the exception of the maxilla and zygo-squamosal (Figure S6A). These bones endured a massive functional change from raptorial feeding in the early toothed mysticetes to filter feeding in the crownward mysticetes[48,49] with change concentrated on a few basal branches, followed by little change within the clade itself.

Suction-feeding cetaceans, such as the ziphiids, also show some of the highest disparity in the skull, which could be due to a relaxation on constraints in morphology when coupled with increased size.[41] In fact, large body size appears to have been selected for in squid-feeding taxa such as ziphiids and sperm whales (*Physeter macrocephalus*).[43] Large suction feeders take in substantial quantities of water, generating adequate suction forces, and thus may not require the shortened rostral morphology of some smaller suction-feeding taxa.[41] Foraging strategy has been highlighted as a major evolutionary driver of diversification in delphinid skull shape[42] and in Odontoceti more generally,[16,40,41,50] as well as a driver of body size.[44] It is, however, important to recognize that although we have characterized all delphinid species except for *Globicephala* and *Grampus* as biting (raptorial) feeders, it has been suggested that all delphinids utilize some combination of raptorial and suction feeding.[40,42] The lack of observational data for most cetaceans makes assignment of feeding strategy categories especially challenging, particularly when categories do not include behavioral frameworks, which are often complex in cetaceans.[51,52] We used broad categories in diet and habitat to help mitigate these uncertainties in ecology and to produce a more robust statistical analysis.

Assignment of habitat categories is similarly challenging, as many cetacean species migrate vast distances, traversing different environments while following migrating food sources or avoiding predation. Nonetheless, we found a clear relationship between skull morphology and habitat type, contra to Galatius et al.,[42] although that study focused primarily on the delphinid skull and noted that adaptations for specific habitats are evident in some subclades, such as the subfamily Lissodelphininae.[42,53] The lowest disparity and generally lower evolutionary rates are observed in the riverine cetaceans, which comprises the three extant freshwater species in this study (*Inia geoffrensis*, *Lipotes vexillifer* [likely recently extinct[54]], and *Platanista gangetica*). The extant river dolphins are the last survivors of their respective families. Possibly marooned in freshwater environments following a reduction in sea levels in the later Miocene, the river dolphins have been largely sheltered from intense competitive pressure that drove a decline in the oceanic delphinoids.[2,55] Convergent morphologies in river dolphin lineages suggest that these cetaceans have successfully adapted to their freshwater niches (including shifts in feeding mode and prey size[25,55,56]), which, coupled with functional constraints of the riverine environment, may result in the low evolutionary rates observed in these taxa.

It should be noted that ecological data for fossils is inferred without direct observation, but is rather based on morphology, isotope geochemistry, tooth microwear, depositional environment, and other correlates of species' ecology. The paleoecological reconstructions used in this study are drawn from previous work focusing on these attributes in extinct whales (Table S1). Other factors of possible interest were wholly excluded due to the inability to estimate them in fossils. For example, we excluded encephalization, or relative brain size, despite its relevance for cranial morphology and other key factors, such as echolocation specifics (and the processing of acoustic data), thermoregulation (e.g., lack of longirostrine morphologies, i.e., increased surface area through which heat can

escape, in colder habitats), and complex social structure—the latter two of which are difficult, if not impossible at present, to study in fossil Cetacea.

The evolution of whales represents an extraordinary transition in ecology, physiology, and anatomy, made even more exceptional by its representation with an exquisite fossil record. Because the cranium captures many of the most extreme shifts in feeding, respiration, and sensory structures, it is ideal for understanding this transition, but no previous study has reconstructed the evolution of the cetacean cranium through the full breadth of their extinct and living diversity. Using a high-resolution geometric morphometric representation of skull shape, we establish the influence of ecology on the evolutionary pace and direction of cetacean cranial evolution and demonstrate that whales achieved their morphological disparity in three key waves of rapid morphological evolution. Future work linking these results with large-scale environmental shifts during the Cenozoic will be pivotal for fully understanding the factors underlying the rise of whales.

## STAR★METHODS

Detailed methods are provided in the online version of this paper and include the following:

- KEY RESOURCES TABLE
- RESOURCE AVAILABILITY
  - Lead contact
  - Materials availability
  - Data and code availability
- EXPERIMENTAL MODEL AND SUBJECT DETAILS
- METHOD DETAILS
  - Digitization
  - Morphometric data collection
  - Phylogeny
  - Ecological traits
- QUANTIFICATION AND STATISTICAL ANALYSIS
  - Cranial variation
  - Patterns of cranial evolution
  - Influences on cranial shape: Allometry and ecology

## SUPPLEMENTAL INFORMATION

Supplemental information can be found online at https://doi.org/10.1016/j.cub.2022.04.060.

## ACKNOWLEDGMENTS

This research was funded by the Natural Environment Research Council Doctoral Training Partnership training grant NE/L002485/1 to E.J.C. E.J.C.'s data collection was also supported by the UCL Bogue Fellowship and the Palaeontological Association Stan Wood Award. This research was also supported by National Science Foundation NSF-EAR 1349607 to J.G., B.B., A.G., and M.C., and University of Wisconsin-Oshkosh Faculty Development Grant to M.C. J.C. was funded by a Marie Skłodowska-Curie Individual Fellowship (IF 797373-EVOTOOLS), T.P. was funded by Leverhulme Research Project Grant (RPG-2019-323), and R.B. was funded by a FRIA fellowship from the F.R.S.-FNRS (grant FC 23645). Special thanks go to Richard Sabin for his help and support throughout and to Erich Fitzgerald for his helpful comments on improving the manuscript and analyses. We would like to thank Anne-Claire Fabre, Carla Bardua, Andrew Knapp, Eve Noirault, Heather White, João Vasco Leite, and Sandra Alvarez-Carretero for their comments, discussion, and help with code and Olivier Lambert, Felix Marx, and Robert Boessenecker for their helpful insights and discussion throughout E.J.C.'s research. Further thanks go to Eve Noirault for help with data collection and digitization of scans. Thanks also go to the many curators and museum staff who helped E.J.C., R.F.B., and M.C. collect scan data. Please see the list of institutions visited in the Github supplemental information. Final thanks go to the anonymous reviewers who helped us to improve the study.

## AUTHOR CONTRIBUTIONS

Conceptualization, E.J.C., A.G., R.N.F., and J.C.; formal analysis, E.J.C., A.G., R.N.F., J.C., and T.P.; investigation, E.J.C., A.G., R.N.F., J.C., and T.P.; methodology, R.N.F., J.C., A.G., and E.J.C.; data acquisition, E.J.C., M.C., R.F.B., J.H.G., and B.B.; writing – review & editing, all authors.

## DECLARATION OF INTERESTS

The authors declare no competing interests.

Received: December 1, 2021
Revised: February 28, 2022
Accepted: April 21, 2022
Published: May 9, 2022

## REFERENCES

1. Gatesy, J., Geisler, J.H., Chang, J., Buell, C., Berta, A., Meredith, R.W., Springer, M.S., and McGowen, M.R. (2013). A phylogenetic blueprint for a modern whale. Mol. Phylogenet. Evol. *66*, 479–506. https://doi.org/10.1016/j.ympev.2012.10.012.
2. Marx, F., Lambert, O., and Uhen, M. (2016). Major steps in the evolution of cetaceans. In Cetacean Paleobiology (Wiley), pp. 157–197.
3. Thewissen, H. (2014). The Walking Whales: From Land to Water in Eight Million Years (University of California Press).
4. Bianucci, G., and Gingerich, P.D. (2011). *Aegyptocetus tarfa*, n. gen. et sp. (Mammalia, Cetacea), from the middle Eocene of Egypt: clinorhynchy, olfaction, and hearing in a protocetid whale. J. Vertebr. Paleontol. *31*, 1173–1188. https://doi.org/10.1080/02724634.2011.607985.
5. Clementz, M.T., Goswami, A., Gingerich, P.D., and Koch, P.L. (2006). Isotopic records from early whales and sea cows: contrasting patterns of ecological transition. J. Vertebr. Paleontol. *26*, 355–370. https://doi.org/10.1671/0272-4634(2006)26[355:irfewa]2.0.co;2.
6. Uhen, M. (2007). Evolution of marine mammals: back to the sea after 300 million years. Anat. Rec. *290*, 514–522.
7. Marx, F., and Fordyce, R. (2015). Baleen boom and bust: a synthesis of mysticete phylogeny, diversity and disparity. R. Soc. Open Sci. *2*, 140434.
8. Heyning, J., and Mead, J. (1990). Evolution of the nasal anatomy of cetaceans. In Sensory Abilities of Cetaceans, J.A. Thomas, and R.A. Kastelein, eds. (Springer), pp. 67–79.
9. Klima, M. (1999). Development of the cetacean nasal skull. Adv. Anat. Embryol. Cell Biol. *149*, 1–143. https://doi.org/10.1007/978-3-642-58612-5.
10. Churchill, M., Geisler, J.H., Beatty, B.L., and Goswami, A. (2018). Evolution of cranial telescoping in echolocating whales (Cetacea: Odontoceti). Soc. Study Evol. *72*, 1092–1108. https://doi.org/10.1111/evo.13480.
11. Roston, R.A., and Roth, V.L. (2019). Cetacean skull telescoping brings evolution of cranial sutures into focus. Anat. Rec. *302*, 1055–1073. https://doi.org/10.1002/ar.24079.
12. Berta, A., Lanzetti, A., Ekdale, E.G., and Deméré, T.A. (2016). From teeth to baleen and raptorial to bulk filter feeding in mysticete cetaceans: the role of paleontological, genetic, and geochemical data in feeding evolution and ecology. Integr. Comp. Biol. *56*, 1271–1284. https://doi.org/10.1093/icb/icw128.

13. Geisler, J.H., Colbert, M.W., and Carew, J.L. (2014). A new fossil species supports an early origin for toothed whale echolocation. Nature *508*, 383–386. https://doi.org/10.1038/nature13086.

14. Churchill, M., Martínez-Cáceres, M., de Muizon, C., Mnieckowski, J., and Geisler, J. (2016). The origin of high-frequency hearing in whales. Curr. Biol. *26*, 2144–2149.

15. Park, T., Fitzgerald, E., and Evans, A. (2016). Ultrasonic hearing and echolocation in the earliest toothed whales. Biol. Lett. *12*, 20160060.

16. Boessenecker, R.W., Fraser, D., Churchill, M., and Geisler, J.H. (2017). A toothless dwarf dolphin (Odontoceti: Xenorophidae) points to explosive feeding diversification of modern whales (Neoceti). Proc. Biol. Sci. *284*, 20170531. https://doi.org/10.1098/rspb.2017.0531.

17. Coombs, E.J., Clavel, J., Park, T., Churchill, M., and Goswami, A. (2020). Wonky whales: the evolution of cranial asymmetry in cetaceans. BMC Biol. *18*. 86–24. https://doi.org/10.1186/s12915-020-00805-4.

18. Steeman, M.E., Hebsgaard, M.B., Fordyce, R.E., Ho, S.Y.W., Rabosky, D.L., Nielsen, R., Rahbek, C., Glenner, H., Sørensen, M.V., and Willerslev, E. (2009). Radiation of extant cetaceans driven by restructuring of the oceans. Syst. Biol. *58*, 573–585. https://doi.org/10.1093/sysbio/syp060.

19. Marx, F.G., and Uhen, M.D. (2010). Climate, critters, and cetaceans: Cenozoic drivers of the evolution of modern whales. Science *327*, 993–996. https://doi.org/10.1126/science.1185581.

20. Jefferson, T., Webber, M., and Pitman, R. (2015). Marine Mammals of the World: A Comprehensive Guide to Their Identification (Academic Press).

21. Bardua, C., Wilkinson, M., Gower, D.J., Sherratt, E., and Goswami, A. (2019). Morphological evolution and modularity of the caecilian skull. BMC Evol. Biol. *19*, 30. https://doi.org/10.1186/s12862-018-1342-7.

22. Felice, R.N., Tobias, J.A., Pigot, A.L., and Goswami, A. (2019). Dietary niche and the evolution of cranial morphology in birds. Proc. Biol. Sci. *286*, 20182677. https://doi.org/10.1098/rspb.2018.2677.

23. Lambert, O., Martínez-Cáceres, M., Bianucci, G., Di Celma, C., Salas-Gismondi, R., Steurbaut, E., Urbina, M., and de Muizon, C. (2017). Earliest mysticete from the late Eocene of Peru sheds new light on the origin of baleen whales. Curr. Biol. *27*, 1535–1541.e2. https://doi.org/10.1016/j.cub.2017.04.026.

24. Geisler, J.H., Boessenecker, R.W., Brown, M., and Beatty, B.L. (2017). The origin of filter feeding in whales. Curr. Biol. *27*, 2036–2042.e2. https://doi.org/10.1016/j.cub.2017.06.003.

25. Geisler, J.H., McGowen, M.R., Yang, G., and Gatesy, J. (2011). A supermatrix analysis of genomic, morphological, and paleontological data from crown Cetacea. BMC Evol. Biol. *11*, 112. https://doi.org/10.1186/1471-2148-11-112.

26. Tsai, C.-H., and Fordyce, R.E. (2018). A new archaic baleen whale *Toipahautea waitaki* (early Late Oligocene, New Zealand) and the origins of crown Mysticeti. R. Soc. Open Sci. *5*, 172453. https://doi.org/10.1098/rsos.172453.

27. Dunn, O.J. (1961). Multiple comparisons among means. J. Am. Stat. Assoc. *56*, 52–64. https://doi.org/10.1080/01621459.1961.10482090.

28. Clavel, J., Escarguel, G., and Merceron, G. (2015). mvMORPH: an R package for fitting multivariate evolutionary models to morphometric data. Methods Ecol. Evol. *6*, 1311–1319. https://doi.org/10.1111/2041-210x.12420.

29. Benjamini, Y., and Hochberg, Y. (1995). Controlling the false discovery rate: a practical and powerful approach to multiple testing. J. R. Stat. Soc. Ser. B Methodol *57*, 289–300.

30. Benjamini, Y., and Yekutieli, D. (2001). The control of the false discovery rate in multiple testing under dependency. Ann. Stat. *29*, 1165–1188. https://doi.org/10.1214/aos/1013699998.

31. Boessenecker, R.W., Churchill, M., Buchholtz, E.A., Beatty, B.L., and Geisler, J.H. (2020). Convergent evolution of swimming adaptations in modern whales revealed by a large macrophagous dolphin from the oligocene of South Carolina. Curr. Biol. *30*, 3267–3273.e2. https://doi.org/10.1016/j.cub.2020.06.012.

32. Lambert, O., Bianucci, G., Post, K., De Muizon, C., Salas-Gismondi, R., Urbina, M., and Reumer, J. (2010). The giant bite of a new raptorial sperm whale from the Miocene epoch of Peru. Nature *466*, 105–108. https://doi.org/10.1038/nature09067.

33. Lipps, J.H., and Mitchell, E. (1976). Trophic model for the adaptive radiations and extinctions of pelagic marine mammals. Paleobiology *2*, 147–155. https://doi.org/10.1017/s0094837300003420.

34. Fitzgerald, E.M.G. (2010). The morphology and systematics of Mammalodon colliveri (Cetacea: Mysticeti), a toothed mysticete from the Oligocene of Australia. Zool. J. Linn. Soc. *158*, 367–476. https://doi.org/10.1111/j.1096-3642.2009.00572.x.

35. de Muizon, C., Bianucci, G., Martínez-Cáceres, M., and Lambert, O. (2019). *Mystacodon selenensis*, the earliest known toothed mysticete (Cetacea, Mammalia) from the late Eocene of Peru: anatomy, phylogeny, and feeding adaptations. Geodiversitas *41*, 401–499. https://doi.org/10.5252/geodiversitas2019v41a11.

36. Fitzgerald, E.M.G. (2006). A bizarre new toothed mysticete (Cetacea) from Australia and the early evolution of baleen whales. Proc. R. Soc. B Biol. Sci. *273*, 2955–2963. https://doi.org/10.1098/rspb.2006.3664.

37. Cardini, A., and Polly, P.D. (2013). Larger mammals have longer faces because of size-related constraints on skull form. Nat. Commun. *4*, 2458. https://doi.org/10.1038/ncomms3458.

38. Randau, M., Sanfelice, D., and Goswami, A. (2019). Shifts in cranial integration associated with ecological specialization in pinnipeds (Mammalia, Carnivora). R. Soc. Open Sci. *6*, 190201. https://doi.org/10.1098/rsos.190201.

39. Vicari, D., Sabin, R.C., Brown, R.P., Lambert, O., Bianucci, G., and Meloro, C. (2022). Skull morphological variation in a British stranded population of false killer whale (Pseudorca crassidens): a three-dimensional geometric morphometric approach. Can. J. Zool. *100*, 119–132.

40. McCurry, M.R., Evans, A.R., Fitzgerald, E.M.G., Adams, J.W., Clausen, P.D., and McHenry, C.R. (2017). The remarkable convergence of skull shape in crocodilians and toothed whales. Proc. R. Soc. B *284*, 20162348. https://doi.org/10.1098/rspb.2016.2348.

41. McCurry, M.R., Fitzgerald, E.M.G., Evans, A.R., Adams, J.W., and McHenry, C.R. (2017). Skull shape reflects prey size niche in toothed whales. Biol. J. Linn. Soc. *121*, 936–946. https://doi.org/10.1093/biolinnean/blx032.

42. Galatius, A., Racicot, R., McGowen, M., and Olsen, M. (2020). Evolution and diversification of delphinid skull shapes. iScience *23*, 101543.

43. Slater, G., Price, S., Santini, F., and Alfaro, M. (2010). Diversity versus disparity and the radiation of modern cetaceans. Proc. R. Soc. B Biol. Sci. *277*, 3097–3104.

44. Sander, P.M., Griebeler, E.M., Klein, N., Juarbe, J.V., Wintrich, T., Revell, L.J., and Schmitz, L. (2021). Early giant reveals faster evolution of large body size in ichthyosaurs than in cetaceans. Science *374*, eabf5787. https://doi.org/10.1126/science.abf5787.

45. Rivin, M.A. (2010). Early Miocene cetacean diversity in the Vaqueros Formation, Laguna Canyon, Orange County, California.

46. Lambert, O., Bianucci, G., and de Muizon, C. (2017). Macroraptorial sperm whales (Cetacea, Odontoceti, Physeteroidea) from the Miocene of Peru. Zool. J. Linn. Soc. *179*, 404–474.

47. Benites Palomino, A., Vélez Juarbe, J., Collareta, A., Ochoa, D., Altamirano, A., Carré, M., Laime, M., Urbina, M., and Salas Gismondi, R. (2021). Nasal compartmentalization in Kogiidae (Cetacea, Physeteroidea): insights from a new late Miocene dwarf sperm whale from the Pisco Formation. Pap. Palaeontol. *7*, spp2.1351.

48. El Adli, J., Deméré, T.A., and Boessenecker, R.W. (2014). *Herpetocetus morrowi* (Cetacea: Mysticeti), a new species of diminutive baleen whale from the Upper Pliocene (Piacenzian) of California, USA, with observations on the evolution and relationships of the Cetotheriidae. Zool. J. Linn. Soc. *170*, 400–466. https://doi.org/10.1111/zoj.12108.

49. Boessenecker, R.W., and Fordyce, R.E. (2017). Cosmopolitanism and Miocene survival of Eomysticetidae (Cetacea: Mysticeti) revealed by

new fossils from New Zealand. New Zealand J. Geology. Geophys. *60*, 145–157. https://doi.org/10.1080/00288306.2017.1300176.

50. Barroso, C., Cranford, T.W., and Berta, A. (2012). Shape analysis of odontocete mandibles: Functional and evolutionary implications. J. Morphol. *273*, 1021–1030. https://doi.org/10.1002/jmor.20040.
51. Hocking, D.P., Marx, F.G., Park, T., Fitzgerald, E.M.G., and Evans, A.R. (2017). A behavioural framework for the evolution of feeding in predatory aquatic mammals. Proc. R. Soc. B Biol. Sci. *284*, 20162750. https://doi.org/10.1098/rspb.2016.2750.
52. Hocking, D.P., Marx, F.G., Park, T., Fitzgerald, E.M.G., and Evans, A.R. (2017). Reply to comment by Kienle (2017b). Proc. R. Soc. B Biol. Sci. *284*, 20171836. https://doi.org/10.1098/rspb.2017.1836.
53. Galatius, A., and Goodall, R.N.P. (2016). Skull shapes of the Lissodelphininae: radiation, adaptation and asymmetry. J. Morphol. *277*, 776–785. https://doi.org/10.1002/jmor.20535.
54. Turvey, S.T., Pitman, R.L., Taylor, B.L., Barlow, J., Akamatsu, T., Barrett, L.A., Zhao, X., Reeves, R.R., Stewart, B.S., Wang, K., et al. (2007). First human-caused extinction of a cetacean species. Biol. Lett. *3*, 537–540. https://doi.org/10.1098/rsbl.2007.0292.
55. Cassens, I., Vicario, S., Waddell, V.G., Balchowsky, H., Van Belle, D., Ding, W., Fan, C., Mohan, R.S.L., Simoes-Lopes, P.C., Bastida, R., et al. (2000). Independent adaptation to riverine habitats allowed survival of ancient cetacean lineages. Proc. Natl. Acad. Sci. USA *97*, 11343–11347. https://doi.org/10.1073/pnas.97.21.11343.
56. Page, C.E., and Cooper, N. (2017). Morphological convergence in 'river dolphin' skulls. PeerJ *5*, e4090. https://doi.org/10.7717/peerj.4090.
57. Lloyd, G.T., and Slater, G.J. (2021). A total-group phylogenetic metatree for Cetacea and the importance of fossil data in diversification analyses. Syst. Biol. *70*, 922–939.
58. R Development Core Team (2020). R: a language and environment for statistical computing (R Foundation for Statistical Computing).
59. Gunz, P., Mitteroecker, P., Neubauer, S., and Weber, G. (2009). Principles for the virtual reconstruction of hominin crania. J. Hum. Evol. *57*, 48–62.
60. Gunz, P., and Mitteroecker, P. (2013). Semilandmarks: a method for quantifying curves and surfaces. Hystrix *24*, 103–109.
61. Cardini, A. (2016). Left, right or both? Estimating and improving accuracy of one-side-only geometric morphometric analyses of cranial variation. J. Zool. Syst. Evol. Res. *55*, 1–10. https://doi.org/10.1111/jzs.12144.
62. Cardini, A. (2016). Lost in the other half: improving accuracy in geometric morphometric analyses of one side of bilaterally symmetric structures. Syst. Biol. *65*, 1096–1106. https://doi.org/10.1093/sysbio/syw043.
63. Fahlke, J.M., Gingerich, P.D., Welsh, R.C., and Wood, A.R. (2011). Cranial asymmetry in Eocene archaeocete whales and the evolution of directional hearing in water. Proc. Natl. Acad. Sci. USA *108*, 14545–14548. https://doi.org/10.1073/pnas.1108927108.
64. Bookstein, F. (1991). Morphometric Tools for Landmark Data: Geometry and Biology (Cambridge University Press).
65. Bookstein, F.L. (1997). Landmark methods for forms without landmarks: morphometrics of group differences in outline shape. Med. Image Anal. *1*, 225–243. https://doi.org/10.1016/s1361-8415(97)85012-8.
66. Bardua, C., Felice, R.N., Watanabe, A., Fabre, A.C., and Goswami, A. (2019). A practical guide to sliding and surface semi landmarks in morphometric analyses. Integr. Org. Biol. *1*, 1–34. https://doi.org/10.1093/iob/obz016.
67. Fahlke, J., and Hampe, O. (2015). Cranial symmetry in baleen whales (Cetacea, Mysticeti) and the occurrence of cranial asymmetry throughout cetacean evolution. Naturwissenschaften *102*, 58.
68. Coombs, E.J., and Felice, R.N. (2021). Quantifying asymmetry in non-symmetrical morphologies, with an example from Cetacea. Preprint at bioRxiv. https://doi.org/10.1101/2021.11.17.468940.
69. Gunz, P., Mitteroecker, P., and Bookstein, F. (2005). Chapter three: semilandmarks in three dimensions. In Modern Morphometrics in Physical Anthropology, D.E. Slice, ed. (Kluwer Academic/Plenum), pp. 73–98.
70. Rohlf, F.J., and Slice, D. (1990). Extensions of the Procrustes method for the optimal superimposition of landmarks. Syst. Zool. *39*, 40–59. https://doi.org/10.2307/2992207.
71. Schlager, S. (2017). Morpho and Rvcg - shape analysis in R. In Statistical Shape and Deformation Analysis, G. Zheng, S. Li, and G. Szekely, eds. (Academic Press), pp. 217–256.
72. de Muizon, C., and Domning, D. (2002). The anatomy of *Odobenocetops* (Delphinoidea, Mammalia), the walrus-like dolphin from the Pliocene of Peru and its palaeobiological implications. Zool. J. Linn. Soc. *134*, 423–452. https://doi.org/10.1046/j.1096-3642.2002.00015.x.
73. Velez-Juarbe, J., Wood, A.R., De Gracia, C., and Hendy, A.J.W. (2015). Evolutionary patterns among living and fossil kogiid sperm whales: evidence from the Neogene of Central America. PLoS One *10*, e0123909. https://doi.org/10.1371/journal.pone.0123909.
74. Collareta, A., Lambert, O., de Muizon, C., Urbina, M., and Bianucci, G. (2017). *Koristocetus pescei* gen. et sp. nov., a diminutive sperm whale (Cetacea: Odontoceti: Kogiidae) from the late Miocene of Peru. Fossil Rec. *20*, 259–278. https://doi.org/10.5194/fr-20-259-2017.
75. Benites-Palomino, A., Vélez-Juarbe, J., Salas-Gismondi, R., and Urbina, M. (2019). Scaphokogia totajpe, sp. nov., a new bulky-faced pygmy sperm whale (Kogiidae) from the late Miocene of Peru. J. Vertebr. Paleontol. *39*, e1728538. https://doi.org/10.1080/02724634.2019.1728538.
76. Peri, E., Collareta, A., and Bianucci, G. (2020). A new record of Physeteroidea from the Upper Miocene of the Pietra leccese (southern Italy): systematics, paleoecology and taphonomy of a fossil macroraptorial sperm whale. Riv. It. Paleontol. Strat. *126*, 751–769.
77. Post, K., and Bosselaers, M. (2005). Late Pliocene occurrence of Hemisyntrachelus (Odontoceti, Delphinidae) in the southern North Sea. DEINSEA *11*, 29–45.
78. Laime Molina, M.J., Urbina Schmitt, M., Chacaltana Budiel, C., and Tejada Medina, L. (2018). Los delfines Lophocetinae (Mammalia: Cetacea: Kentriodontidae) de la formación pisco de cerro yesera de amara, Ocucaje, Ica, pp. 47–50.
79. Lambert, O., Godfrey, S.J., and Fitzgerald, E.M.G. (2018). *Yaquinacetus meadi*, a new latest Oligocene–early Miocene dolphin (Cetacea, Odontoceti, Squaloziphiidae, fam. nov.) from the Nye Mudstone (Oregon, U.S.A.). J. Vertebr. Paleontol. *38*, e1559174. https://doi.org/10.1080/02724634.2018.1559174.
80. Rosel, P.E., Wilcox, L.A., Yamada, T.K., and Mullin, K.D. (2021). A new species of baleen whale (*Balaenoptera*) from the Gulf of Mexico, with a review of its geographic distribution. Mar. Mamm. Sci. *37*, 577–610. https://doi.org/10.1111/mms.12776.
81. Berta, A., and Lanzetti, A. (2020). Feeding in marine mammals: an integration of evolution and ecology through time. Palaeontol. Electron. *23*, 4. https://doi.org/10.26879/951.
82. Adams, D., Collyer, M., and Kaliontzopoulou, A. (2020). Geomorph: software for geometric morphometric analyses. R package version 3.2.1. https://cran.r-project.org/package=geomorph.
83. Revell, L.J. (2012). Phytools: an R package for phylogenetic comparative biology (and other things). Methods Ecol. Evol. *3*, 217–223. https://doi.org/10.1111/j.2041-210x.2011.00169.x.
84. Pagel, M. (1997). Inferring evolutionary processes from phylogenies. Zool. Scr. *26*, 331–348. https://doi.org/10.1111/j.1463-6409.1997.tb00423.x.
85. Pagel, M. (1999). Inferring the historical patterns of biological evolution. Nature *401*, 877–884. https://doi.org/10.1038/44766.
86. Gelman, A. (2006). Prior distributions for variance parameters in hierarchical models (comment on article by Browne and Draper). Bayesian Anal. *1*, 515–534. https://doi.org/10.1214/06-ba117a.
87. Gelman, A., and Rubin, D. (1992). Inference from iterative simulation using multiple sequences. Stat. Sci. *7*, 457–472.
88. Plummer, M., Best, N., Cowles, K., and Vines, K. (2006). CODA: convergence diagnosis and output analysis for MCMC. R News *6*, 7–11.
89. Ferguson-Gow, H. (2020). BTprocessR: a set of tools to help with the interpretation and analysis of the output of BayesTraits MCMC analyses.

90. Xie, W., Lewis, P.O., Fan, Y., Kuo, L., and Chen, M.H. (2011). Improving marginal likelihood estimation for bayesian phylogenetic model selection. Syst. Biol. *60*, 150–160. https://doi.org/10.1093/sysbio/syq085.

91. Venditti, C., Meade, A., and Pagel, M. (2011). Multiple routes to mammalian diversity. Nature *479*, 393–396. https://doi.org/10.1038/nature10516.

92. Felice, R. (2021). Macroevo plots in R. https://github.com/rnfelice/macroevo.plots/tree/master/R.

93. Wang, L.G., Lam, T.T.Y., Xu, S., Dai, Z., Zhou, L., Feng, T., Guo, P., Dunn, C.W., Jones, B.R., Bradley, T., et al. (2020). Treeio: an R package for phylogenetic tree input and output with richly annotated and associated data. Mol. Biol. Evol. *37*, 599–603. https://doi.org/10.1093/molbev/msz240.

94. Bardua, C., Fabre, A.C., Clavel, J., Bon, M., Das, K., Stanley, E.L., Blackburn, D.C., and Goswami, A. (2021). Size, microhabitat, and loss of larval feeding drive cranial diversification in frogs. Nat. Commun. *12*, 2503. https://doi.org/10.1038/s41467-021-22792-y.

95. Guillerme, T., and Weisbecker, V. (2019). landvR: tools for measuring landmark position variation (Zenodo). https://doi.org/10.5281/zenodo.2620785.

96. Clavel, J., Aristide, L., and Morlon, H. (2019). A penalized likelihood framework for high-dimensional phylogenetic comparative methods and an application to new-world monkeys brain evolution. Syst. Biol. *68*, 93–116. https://doi.org/10.1093/sysbio/syy045.

97. Clavel, J., and Morlon, H. (2020). Reliable phylogenetic regressions for multivariate comparative data: illustration with the MANOVA and application to the effect of diet on mandible morphology in phyllostomid bats. Syst. Biol. *69*, 927–943. https://doi.org/10.1093/sysbio/syaa010.

## STAR★METHODS

### KEY RESOURCES TABLE

| REAGENT or RESOURCE | SOURCE | IDENTIFIER |
|---|---|---|
| Deposited data | | |
| Trees for all phylogenetic analyses | https://github.com/EllenJCoombs/Cetacean_cranial_evolution | N/A |
| | Lloyd and Slater[57] | N/A |
| 3D surface scans | https://www.phenome10k.org/ | N/A |
| | https://www.morphosource.org/<br>https://sketchfab.com/ | N/A |
| Software and algorithms | | |
| BayesTraitsV3 | http://www.evolution.rdg.ac.uk/ | N/A |
| R Studio v. 3.5.0 | R Core Team[58] | N/A |

### RESOURCE AVAILABILITY

#### Lead contact

Further information and requests for resources should be directed to and will be fulfilled by the lead contact, Ellen Coombs (ellen.coombs.14@ucl.ac.uk).

#### Materials availability

3D scan data available at: https://www.phenome10k.org/, https://www.morphosource.org/, or https://sketchfab.com/. For scans not available on these sites (for example, material that is not yet described) please contact Ellen Coombs (ellen.coombs.14@ucl.ac.uk or the corresponding museum curator).

#### Data and code availability

All original code is available at https://doi.org/10.5281/zenodo.6506812 and is publicly available as of the date of publication. DOIs are listed in the key resources table. All R package version details available at: https://github.com/EllenJCoombs/Cetacean_cranial_evolution.

Any additional information required to reanalyze the data reported in this paper is available from the lead contact upon request.

### EXPERIMENTAL MODEL AND SUBJECT DETAILS

Our data set comprises stem cetaceans (archaeocetes, n = 11), and members of both extant suborders: baleen whales (mysticetes, n = 33) and toothed whales (odontocetes, n = 157). The final data set includes 201 cetacean crania, of which 113 (56%) are extinct, ranging in age from 48.6 Mya to 2.59 Mya. We selected specimens to cover the widest possible phylogenetic breadth, representing 41 families, 122 genera, and ~95% of extant species (Table S1).

Due to the use of 3D geometric morphometric data for the entire cranium, sampling was limited by specimen completeness and preservation. Inclusion of fossil specimens was determined by the extent of deformation and missing data. Eighty-seven (43%) of the specimens, including some extant taxa, had missing data which was concentrated in the pterygoid, palate, jugal, squamosal, and tip of the rostrum. Specimens with obvious taphonomic or other deformation were excluded from further analysis. Sexual dimorphism was not considered in this study as most fossils and many extant specimens lack data on sex. All specimens are adults except for *Mesoplodon traversii* (NMNZ TMP012996) which is a sub-adult.

### METHOD DETAILS

#### Digitization

Skulls were scanned using a Creaform Go!SCAN 20, Creaform Go!SCAN 50, Artec Eva white light, or a Creaform Handyscan laser scanner, depending on the size of the skull. Scans were initially cleaned, merged, and exported in ply format using VXElements v.6.0, and further cleaned and decimated in Geomagic Wrap software (3D Systems). Models were decimated down to 1,500,000 triangles, reducing computational demands, while retaining sufficient detail for morphometric analysis. In many morphometrics studies, it is possible to digitally reconstruct bilateral elements by mirroring across the midline plane if the skull (or object) is preserved on one side.[59–62] Due to a natural asymmetry occurring in the archaeocete and odontocete skull,[17,63] mirroring was limited to marginally damaged bones or bilaterally symmetric structures[17] using the 'mirror' function in Geomagic Wrap 2017 (3D Systems).

### Morphometric data collection

We placed 123 landmarks and 124 curve sliding semi-landmarks on each specimen using Stratovan Checkpoint (Stratovan, Davis, CA, USA) (Tables S2 and S3; Figure SA: https://github.com/EllenJCoombs/Cetacean_cranial_evolution). Landmarks were defined as Type I (biology) or Type II (geometry)[64,65] and were chosen to capture clear definitions e.g., tripartite sutures. Sliding semi-landmark curves (hereafter termed 'curves') define key structures such as the margins of bones and anatomical ridges, representing a significant increase in shape capture compared to landmark-only data sets.[65,66]

Archaeocetes have prevalent asymmetry in the rostrum and in the squamosal, jugal, and orbit, and, although some of this may represent preservational deformation, it is possible that some is biological.[17,63] Asymmetry in odontocetes is predominant in the naso-facial region, whilst mysticetes show a high degree of symmetry similar to terrestrial artiodactyls.[17,67] Due to these differences in asymmetry among suborders, asymmetric elements were manually landmarked on both sides of the skull, while symmetric elements were mirrored using the using the mirrorfill function in the R package 'paleomorph' v.0.1.4 (for methodological details and code, see Coombs and Felice[68]). The resulting data set is identical in terms of landmarks and curves across all suborders, allowing unified analyses across the whole of Cetacea[68] (Figure SA, as above).

Following manual placement, semi-landmark curves were each resampled to a consistent number across specimens (Table S3; Figure SB: https://github.com/EllenJCoombs/Cetacean_cranial_evolution) and then slid to minimize bending energy.[66,69] Following sliding, all morphometric data were subjected to Procrustes superimposition to remove variation due to orientation (both rotation and translation) and isometric size.[70] Log centroid size, extracted from cranial shape data during Procrustes superimposition, was used in further analyses as a proxy of overall size (Table S4).

Although sampling was limited to specimens that were undeformed and mostly complete, there were some instances of missing elements or structures. Where structures were missing due to preservation, rather than true biological absence, the relevant landmarks and semi-landmarks were estimated with fixLMtps function from the R package 'Morpho,'[71] which uses weighted averages from the three most morphologically similar, complete, configurations to estimate missing landmarks for the incomplete missing specimen. Where structures were genuinely absent, for example in *Odobenocetops*, a bizarre walrus-like whale from the Pliocene of Peru in which the maxilla lacks a ventral exposure,[72] the entirely absent nasals in Kogiidae,[73–75] and the absent right nasal in physeteroids (except *Acrophyseter*),[76,46] all relevant landmarks and semi-landmarks were placed in a single "zero-area" point adjacent to its position in other taxa, following the method described by Bardua et al.[66] In all specimens, the lacrimal was included in the lateral process of the maxilla (anterior rim of the orbit) due to its variable development and relative featurelessness in neocetes.[2] Further, the squamosal includes a well-developed anteriorly directed process, the zygomatic process,[2] which is included here as one element called the 'zygo-squamosal,' and the mandibular process includes the mandibular fossa and surrounding process. See Table S2 for details. Finally, in species with extreme maxillary crests (e.g., *Platanista gangetica* and *Hyperoodon ampullatus*), landmarks and semi-landmarks were placed under or around the crests as not to include them and skew the results (for figures see https://github.com/EllenJCoombs/Cetacean_cranial_evolution).

### Phylogeny

The phylogenetic framework for all analyses in this study modifies a recent comprehensive analysis from Lloyd and Slater[57] by adding the following specimens: *Hemisyntrachelus oligodon* (SMNK-PAL 3841) was placed in the same genus as *Hemisyntrachelus cortesii*[77] MUSM 605 and MUSM 563 were ascribed to the subfamily, Lophocetinae, as sister taxa to *Macrokentriodon*;[78] *Yaquinacetus* sp. (USNM 214705) was placed in the Squaloziphiidae, as in Lambert et al.,[79] near to the *Chilcacetus* clade, which includes *Chilcacetus cavirhinus* (MUSM 1401; also in this study). Finally, *Scaphokogia totajpe* was placed in the same genus as *Scaphokogia cochlearis*, following Benites-Palomino et al.[75] *Balaenoptera ricei* was placed according to Rosel et al.[80]

### Ecological traits

Five ecological or ecomorphological traits relevant to feeding and sensory functions of the cranium were scored from the primary literature, as well as categories established in previous studies[41,51,52,81] (Table S1). Given the breadth of species in this data set, as well as inevitable uncertainties on ecology and life history for many species, and the need for a minimum of five species in each bin for statistical analyses, we used relatively broad categories to capture diet and habitat.

#### *Dentition*

Dentition was divided into four categories: homodont, heterodont, reduced, and edentulous. 'Reduced' dentition includes suction feeders such as ziphiids which are characterized by a decreased number of teeth relative to the heterodont or homodont condition. 'Edentulous' species are characterized by their lack of functional teeth and in many, but not all, cases possess baleen.[81]

#### *Diet*

Diet was divided into five categories: 'fish', 'benthic invertebrates and fish', 'cephalopods and fish', 'tetrapods + fish', 'zooplankton and fish'. In the latter four categories, fish make up a substantial but minority component of the diet.

#### *Echolocation ability*

Echolocation ability was divided into two categories: all non-echolocating cetaceans (archaeocetes and mysticetes), and echolocating cetaceans (all odontocetes apart from *Odobenocetops*).[2,72] Scorings for fossil taxa were based on species-specific reconstructions in the literature (Table S1). Although finer categories are possible, they bring substantial uncertainty in scoring, particularly with fossil data.

### *Feeding method*

Feeding method was divided into three categories: biting, suction, and filter feeding. As with the other traits, feeding behaviors are difficult or impossible to establish for fossils and thus finer categories are not used here. Where possible, species scores follow Hocking et al.,[51,52] which incorporates experimental models and observational data from extant taxa onto their estimates for extinct species.

### *Habitat*

Habitat was categorized as: riverine (freshwater), coastal, coastal-pelagic, or pelagic and based on categories used in Jefferson et al.[20] and Berta and Lanzetti.[81]

## QUANTIFICATION AND STATISTICAL ANALYSIS

### Cranial variation

Principal component analysis (PCA) of Procrustes-transformed morphometric data was used to assess the primary aspects of shape variation and morphospace occupation for the cranium. Morphologies representing the extreme shapes along the principal component (PC) axes were generated to visualize shape variation. We further conducted a phylogenetic principal component analysis, and phylogenetic PC scores (pPC scores) representing 95% of the total variation were extracted and used in further analyses to reduce data dimensionality. PCA was conducted using the 'gm.prcomp' function in the R package 'geomorph' v.3.3.1[82] and pPC scores calculated using the 'phyl.pca' function in the R package 'phytools'[83] v.0.7-70. Thirty-nine phylogenetically corrected principal components (pPC) scores captured 95% of the variation in skull shape across Cetacea (Table S4). Between three and 30 pPC scores were required to represent the bones and skulls across the different suborders (Table S4).

### Patterns of cranial evolution

We investigated branch-specific evolutionary rates and rates through time with a reversible-jump Markov Chain Monte Carlo (rjMCMC) algorithm in BayesTraitsV3 (http://www.evolution.rdg.ac.uk/) for the entire skull and for individual bones, using the pPC scores that represent 95% of the shape variation for the relevant structure (Table S5). We first compared support for single and variable rate Brownian Motion models (BM) with kappa (a measure of punctuated evolution), delta (indicating an increase or decrease in the rate of evolution through time such as an 'early-burst' model), and lambda (a measure of phylogenetic signal in which the shared history of taxa drives trait distribution at the tips[84,85]) tree transformations, as well as Ornstein-Ulenbeck models. All models were run with both single and variable rates, resulting in a total of 10 tested models (Figure S3).

We assessed for convergence of the chains by visually assessing the trace plots and then checking the effective sample size (ESS) with Gelman and Rubin's diagnostics,[86,87] using the 'effectiveSize' and 'gelman.diag' functions implemented in the R package 'coda' v.0.19-4[88] (Figure S7). If the runs had not converged successfully, longer MCMC chains were run. Convergence was achieved using 200 million iterations and a burn-in of 20 million, sampling every 20,000 iterations for the whole skull data set and all bones. A stepping-stone sampler was used to estimate marginal likelihood for each model setting 500 stones to each run for 5000 iterations, with results processed using BTProcessR.[89,90] Based on Bayes Factor, the best model fit for all elements and the whole skull was the lambda model with variable rates (Lambda_var)[91] (Figure S3).

Rate shifts with posterior probabilities > 0.6 and branch-specific rates were visualized for the best supported model. Average evolutionary rates were plotted through time for the whole cranium across Cetacea, for each suborder, for each cranial bone across Cetacea, and for each suborder using the rttplotter function and the mytreebybranch function from Felice[92] and the R package 'treeio.'[93] Mean log rates per family were also plotted using the rjpp output from BayesTraits. Several specimens are categorized as '*incertae sedis*' as they have not yet been formally assigned to a family and thus, they were not included in the plots showing family rates (Table S1). Finally, the output from BTRTools was used to construct density plots to compare evolutionary rates between suborders and families[92] (Figure 3).

We further compared evolutionary rates among clades (archaeocetes, mysticetes, and odontocetes) and ecological categories (diet, dentition, feeding type, echolocation, and habitat) using the pPC scores that represented the whole cranium. For each analysis, we first used stochastic character mapping implemented in the 'make.simmap' function in 'phytools' with an 'ARD' model to sample 100 possible evolutionary histories for each ecological variable's states and transitions between each suborder. We summarized these sampled character state histories for each variable using a custom function (paintAllTree, see https://github.com/EllenJCoombs/Cetacean_cranial_evolution). We then applied the state-specific Brownian Motion (BMM) model in the 'mvgls' function in mvMORPH v.1.1.4[28] with the option 'error = TRUE' to mitigate sources of evolutionary rates inflation, including departures from Brownian Motion caused by measurement error and any intra-specific variation (see e.g., Bardua et al.[94]).

We further calculated disparity (Procrustes variance) for each cranial element and for the whole skull, for each of the suborders and for Cetacea as a whole, using the 'morphol.disparity' function in geomorph.[82] To directly compare across bones, we scaled total disparity by the number of landmarks and semi-landmarks for each bone and compared disparity among ecological groups. We further visualized disparity in the skull using the R package 'landvR' v.0.4[95] to calculate the Procrustes distance from the mean skull shape for a selection of key families representing early, middle, and late (including all extant mysticetes and odontocetes) members of each suborder.

### Influences on cranial shape: Allometry and ecology

We used log centroid size and Procrustes coordinates to estimate the contribution of allometry (size-related shape variation) to overall variation in skull shape across Cetacea, using the procD.lm function in geomorph. We then used phylogenetic MANOVAs to quantify the associations among cranial shape and centroid size, dentition, diet, feeding method, echolocation ability, and habitat.

We ran Chi-squared tests ($\chi^2$) to assess if some predictors were perfectly collinear due to the nested nature of the categorical variables related to diet, feeding, foraging, and feeding apparatus. We found that there was a strong relationship between all variables except for echolocation ability and habitat ($\chi^2 = 8.509$, $p = 0.484$). Due to the clear relationships (i.e., the nested nature of the variables) between dentition, diet, feeding method, and echolocation, we did not run pMANOVAs with interactions. As there was no clear relatedness between echolocation ability and habitat, we ran a pMANOVA with interactions for these variables and found that there was no strong effect of an interaction between them on skull shape ($F = 1.6009$, $p = 0.09$).

We ran these Type II pMANOVAs in mvMORPH[28] using the pPC scores and applying the mvgls and manova.gls commands with Pagel's lambda and using penalized likelihood for model fit. The significance of each predictor was assessed with Pillai's statistic and 1000 permutations.[96,97] This flexible approach accommodates departures from single rate Brownian Motion models. We accounted for false discovery rate using the Benjamini-Hochberg correction.[29,30] All analyses were carried out in R v. 3.5.0.[97]